

# Frozen-in photoconductivity in PbTe:O films

K. A. Baklanov and I. P. Krylov

*Kapitza Institute of Physics Problems, USSR Academy of Sciences*

(Submitted 10 July 1991)

*Zh. Eksp. Teor. Fiz.* **101**, 294–326 (January 1992)

We investigated the preservation of high photoconductivity of oxidized PbTe films for a long time after turning off the light, at temperatures  $T \lesssim 100$  K. The film conductivity  $G$  was measured as a function of the time  $t$  under exposure and relaxation conditions. A logarithmic variation  $\Delta G \propto \log t$  was observed in both cases. The experimental results were analyzed using the solution of a kinetic equation in which the initial parameters were the cross sections  $\sigma_1$  and  $\sigma_2$  for photoionization of the primary photosensitive centers and the metastable traps, as well as the conduction-electron trapping time  $\tau$ . For agreement with experiment, distributions of the centers in cross section  $\sigma'_1 < \sigma_1 \leq \sigma''_1$  and of the traps in time  $\tau_1 \leq \tau < \tau_2$  were introduced, with distribution functions  $dn/d\sigma_1 \propto \sigma_1^{-1}$  and  $dn/d\tau \propto \tau^{-1}$ . All the numerical values of the parameters were determined and found to agree with the theoretical estimates. The second-illumination method was used to establish the existence of a deep-center metastable state due to a strong vibronic interaction. An exhaustive investigation of the photoconductivity relaxation led to the conclusion that trapping of nonequilibrium electrons is a process similar to Anderson localization. The size of the trap formed as a superposition of atomic states of individual defects is determined from the ionization cross section  $\sigma_2 \approx 10^3 \sigma'_1$ . It is shown by the method of intermediate annealing that  $\sigma_2$  decreases smoothly with increase of the trap annealing time  $T_i$  and tends at  $T_i > 100$  K to the value  $\sigma''_1 \approx 10^{-17}$  cm<sup>2</sup>, typical of deep centers in PbTe:O.

## INTRODUCTION

When PbTe films oxidized under normal atmospheric conditions and cooled to  $T = 4.2$  K are illuminated their conductivity increases by several orders.<sup>1</sup> When the light is turned off the conductivity remains high for an indefinitely long time. We call this frozen-in photo-conductivity (FPC), with emphasis on the role of the low temperature.

Persistent photoconductivity has been known for a long time. It was observed in many semiconductors at low as well as at room temperature (see the reviews<sup>2,3</sup>). In most cases this phenomenon was attributed to microscopic or macroscopic energy barriers in the sample, separating in space the nonequilibrium carriers. The barrier height determined the carrier-recombination time scale. Lang<sup>4</sup> proposed in 1977 a less trivial mechanism connected with vibronic interaction. A change of the charge state of the defect in which a free carrier is localized deforms the lattice around this center, referred to as "deep." The result is an energy barrier, due to lattice-ion motion, to localization of nonequilibrium carriers. The barrier is the elastic energy of lattice deformation. It is this mechanism which we regard as crucial for the explanation of FPC in PbTe:O films, although the spatial separation of the charges plays a role of its own.

We emphasize that in the entire paper we attribute the change of the conductivity  $G$  exclusively to changes of the free-carrier density, assuming a constant carrier mobility. This premise is used to have a definite interpretation of the results in agreement with Mott's approach for disordered conductors.

The alloying fluctuations spontaneously produced when the films were prepared created a random potential for the carriers. This brought about the Anderson-localization conditions, and we dealt with the insulator side of the metal-insulator junction. The nonequilibrium-carrier trapping investigated here in detail enables us to consider Anderson

localization from a new viewpoint. We can, for example, compare the localization radius  $r_T$  with the cross section  $\sigma_2$  for trap photoionization. As seen in the experiments described below,  $\sigma_2$  decreased smoothly with rise of the annealing temperature of states localized in a random relief. The problem of Anderson localization in lead telluride is made complicated not only by the electron-electron interaction, but also by a vibronic interaction that alters the equilibrium positions of the lattice ions in the course of the localization.

Lead chalcogenides are narrow-gap semiconductors. According to the tabulated data, the band gap of PbTe is  $E_g = 0.188$  eV at  $T = 4.2$  K and increases linearly to  $E_g = 0.31$  eV at  $T = 300$  K (Ref. 5). The carrier effective masses range between 0.02 and 0.2 of the free-electron mass  $m_0$ . We shall use the averaged value  $m^* = 0.05 m_0$  contained in the equation for the density of states and is approximately the same for electrons and ions. The static dielectric constant of lead tellurite is  $\epsilon \approx 1000$  at  $T = 4.2$  K and the refractive index in the optical band is  $\eta \approx 6$ . The density of the intrinsic carriers is  $n_i \approx 10^{16}$  cm<sup>-3</sup> at  $T = 300$  K. Lead tellurite has an NaCl-type crystal structure with a lattice constant  $a = 6.46$  Å. The Debye temperature is  $\Theta \approx 140$  K.

It is known that in pure A<sup>4</sup>B<sup>6</sup> semiconductors the carrier density and type are determined by the deviation from stoichiometry.<sup>6</sup> An onset of donors is ensured by an excess of group-IV metals, designated as A<sup>4</sup>, while acceptors are produced by an excess B<sup>6</sup> of chalcogens. Deviations from stoichiometry in PbTe crystals are due to lattice point defects, mainly vacancies, which are deep centers.<sup>7</sup> This means that local electronic vacancy levels lie far from band edges. Shallow hydrogenlike impurity levels cannot localize carriers in view of the extremely low binding energy  $E_H \sim m^* e^4 / \hbar^2 \epsilon^2 \sim 10^{-6}$  eV and correspondingly large radius  $a_H \sim \epsilon \hbar^2 / m^* e^2 \sim 10^{-4}$  cm of the hydrogenlike center. The vacancy short-range potential is not screened by the polarization of the electron shells that ensure a large value of  $\epsilon$ .

The local-level binding energy turns out therefore to be comparable with the band gap  $E_g$ .

Many experiments<sup>6</sup> have shown that carriers are not frozen out in  $A^4B^6$  chalcogenides. For example, even in pure PbTe crystals the Hall constant depends little on temperature down to 4.2 K. Calculations<sup>7,8</sup> show that local vacancy levels break far away from the band states that generate them. Lead vacancies are thus doubly ionized acceptors and produce acceptor levels in the valence band of a PbTe crystal, while the tellurium vacancies are doubly charged donors, with the majority of donor levels located in the conduction band. This explains fully the metallic character of the temperature dependences of the conductivity and of the Hall constant in PbTe crystals.

According to theory,<sup>7</sup> one of the tellurium vacancy levels, which we label  $E_0^*$ , is close to the bottom of the conduction band. To determine their relative position it is necessary to take into account more subtle effects of the interaction with the lattice, particularly the Jahn–Teller effect.<sup>9</sup> The outer electron shells include the states  $5s^25p^4$  for Te and  $6s^26p^2$  for Pb. It is assumed that the  $s$  states form bonds having very deep levels and do not take part in the phenomena of interest to us. The wave functions of electrons localized on a point defect are therefore superpositions of  $p$ -orbitals that transform in accordance with the irreducible vector representation  $\Gamma_{15}^-$  of the cube group. The state  $E_0^*$  should therefore be a triply degenerate term that is split by the spin orbit interaction into a singlet  $\Gamma_6^-$  and a doublet  $\Gamma_8^-$  in accordance with the relation  $\Gamma_{15}^- \times D_{1/2} = \Gamma_6^- + \Gamma_8^-$ . Perturbation of the periodic lattice potential upon formation of a vacancy corresponds to repulsion. Therefore  $\Gamma_8^-$  lies lower than  $\Gamma_6^-$ . Electron trapping in a degenerate  $\Gamma_8^-$  state on account of Jahn–Teller instability should be accompanied by a lattice deformation that lowers the symmetry of the crystalline surrounding of the vacancy and lifts the degeneracy. The energy level of an electron localized on a tellurium vacancy can then turn out to be lower than the Fermi level  $E_f$ , as against  $E_0^+ > E_f$  prior to localization. The authors of Ref. 9 assume correctly that this phenomenon should lead to frozen-in photoconductivity. In fact, persistent relaxations were observed in  $Pb_{1-x}Sn_xTe$ :In alloys perturbed by light<sup>10</sup> or by a magnetic field,<sup>11</sup> and the parameters of a Jahn–Teller center are given in Ref. 12. So far, however, frozen-in conductivity has not been observed in pure PbTe crystals or  $\epsilon$ lms.

## SPECIMENS

The PbTe films were obtained by condensing the telluride vapor on a glass substrate at room temperature. The initial PbTe powder was sublimated from a tantalum evaporator in vacuum at a residual-gas pressure  $p < 10^{-5}$  Torr. The initial high-purity substance had an impurity density  $\sim 10^{15} \text{ cm}^{-3}$ . It is known<sup>13</sup> that at a sublimation temperature  $\approx 800^\circ\text{C}$  the deviation from stoichiometry is of the order of  $10^{-3}$ . The mass  $M$  of the precipitated matter was determined from the frequency shift of a quartz cavity located alongside the substrate. Using the known density  $\rho = 8.2 \text{ g/cm}^3$  of the PbTe crystals, we determined from  $M$  the film thickness  $d$ . In separate experiments, measuring the film thickness with a microinterferometer, Poyarkov<sup>14</sup> found that the matter density in the precipitated film is  $p_n \approx 0.7p$ .

TABLE I.

Sample No.	Thickness, $\text{\AA}$	$\rho(300\text{K}), (\Omega \cdot \text{cm}^{-1})$	$\rho(300\text{K})/\rho(77\text{K}), 10^3$
1	950	0,58	14
2	1300	1,4	11
3	414	0,91	120
4	1000	0,59	15

In our experiments we used about 30 specimens with  $d = 200\text{--}2000 \text{ \AA}$ . Most of the results discussed below were obtained for the four numbered specimens whose main characteristics are listed in Table I.

Debyegrams of several films were obtained with an x-ray diffractometer. The lattice constant  $a$  determined from these data agreed with the tabulated data. The widths of the diffraction peaks corresponded to the pattern of a polycrystalline specimen with crystallites measuring  $\sim 1000 \text{ \AA}$ . About ten films with different thicknesses were studied with a scanning electron microscope (SEM). Figure 1 shows two microphotographs of a section of the surface of one of the films. In the SEM investigations we used the potential- and material-contrast methods. In the first case we used a detector of secondary electrons of energy  $< 50 \text{ eV}$ , reacting to changes  $\delta U \lesssim 1 \text{ V}$  of the sample-surface potential. In the material-contrast method a detector was included for the reflected electrons with energy close to the  $\sim 10 \text{ keV}$  of the incident beam. In this case small  $\delta U$  do not influence the SEM signal. At the same time the electron reflection coefficient  $R_e$  increases with the atomic number  $Z$  of the element located within  $< 1000 \text{ \AA}$  from the specimen surface. The relation  $R_e \propto Z$  for light elements is replaced at  $Z \gtrsim 50$  by a weaker dependence, so that the sensitivity of the material-contrast method to the specimen composition is low. In both SEM signal registration methods, however, the most important factor influencing the contrast is the topographic relief of the specimen surface. Thus, Fig. 1b reveals small surface irregularities but no alloying variations. On the contrary, Fig. 1a shows a variation of the potential along the film, obviously corresponding to alloying irregularities, i.e., ran-

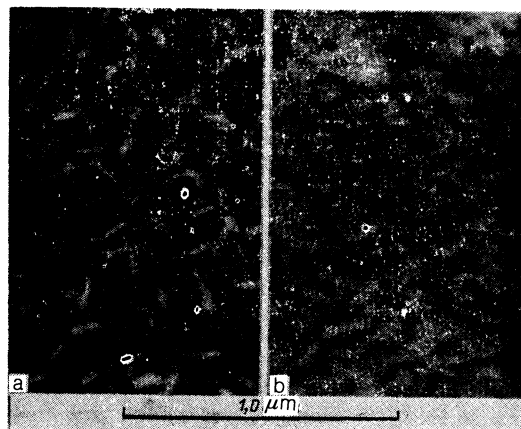


FIG. 1. Surface microphotographs of PbTe film  $1200 \text{ \AA}$  thick: a—potential contrast, b—topographic relief (material contrast). The frame borders are the same in both photographs.

dom alternation of  $p$ - $n$  regions. Negatively charged  $p$ -regions correspond to white "worms" on the photograph, and positive  $n$ -regions to the relatively uniform dark background. Attention is called to the small scatter of the sizes of the  $p$ -regions. The ratio of the "worm" dimensions was on the average  $b_1:b_2 \approx 3:1$  with  $b_2 \approx 300 \text{ \AA}$ . In Fig. 1b there are clearly pronounced dark spots measuring  $\sim 1000 \text{ \AA}$ , which can be tracked also in the corresponding spots on Fig. 1a. We assume that these are pores passing through the entire film. The basis for this conclusion is the value  $\rho_n/\rho < 1$ . In addition, experiments<sup>15</sup> with layered Pb-PbTe-Pb structures have shown a frequent onset of metallic "short circuits" passing through the PbTe film.

In all cases, an SEM study of PbTe:O films yielded a similar picture. The number of bright  $p$  regions on thin ( $d < 400 \text{ \AA}$ ) films was much smaller, i.e., the films were more uniform. Thick ( $d \approx 2000 \text{ \AA}$ ) films showed  $b_1$  and  $b_2$  approximately 1.5 times larger. No structure inhomogeneities of larger scale were noted. Observation of the specimens visually or with an optical microscope showed the uniform mirror surface typical of good metallic films. This metallic appearance does not change when the film is cooled. Recognizing that  $\hbar\omega \gg E_g$  for visible light, it is natural to assume that the optical properties of PbTe are close to the properties of a metal with a carrier density 3 electrons/atom, determined by the average number of valent  $p$ -electrons.

Certain experiments with oxidation of PbTe films were performed by Poyarkov.<sup>14</sup> The vacuum system was capable of cooling a freshly deposited film to  $T \approx 80 \text{ K}$  without exposing it to atmospheric air. In accord with the results of Ref. 16, it turned out that the conductivity  $G$  at  $T = 300 \text{ K}$  and its temperature variation  $G(T)$  depend strongly on the degree of oxidation. The conductivity of a freshly deposited non-oxidized film was changed no more than 50% by cooling from 300 K to 80 K, in accord with the published data for PbTe crystals.

Admission of oxygen into the volume containing a film at  $T = 80 \text{ K}$  increased the film resistance, but evacuation of the oxygen restored the initial resistance. An irreversible increase of resistance was produced if the film was at room temperature. At a pressure  $p_{O_2} \approx 1 \text{ Torr}$  the appreciable resistance changes were completed after several minutes. We assume that the oxygen density in the film has practically reached saturation in this case. Poyarkov's measurements of PbTe:O films coated on a quartz cavity have shown that the oxygen mass absorbed in the film is proportional to its thickness. For a uniform distribution of the oxygen admixture, the data lead to the unjustifiably large saturation density  $n_0 > 10^{20} \text{ cm}^{-3}$ . As noted in Ref. 14, the overestimate of  $n_0$  is due to the porosity of the films which absorb macroscopic  $O_2$  layers on the surfaces of the pores.

One of our oxidized PbTe films was subjected at the Semiconductor Chemistry and Physics Laboratory of the Moscow State University<sup>1)</sup> to an Auger analysis that revealed the presence of the elements Pb, Te, O, and C. A plasma scrubbing of all the surface contaminations removed the traces of oxygen as well as carbon. The low sensitivity of the analysis ( $\sim 3\%$ ) made it impossible to determine the density of the O impurity in the PbTe matrix. It can be asserted, however, with the same degree of accuracy, that no inclusions of a pure phase of any chemical compound with oxygen in its molecule have been produced in the oxidized

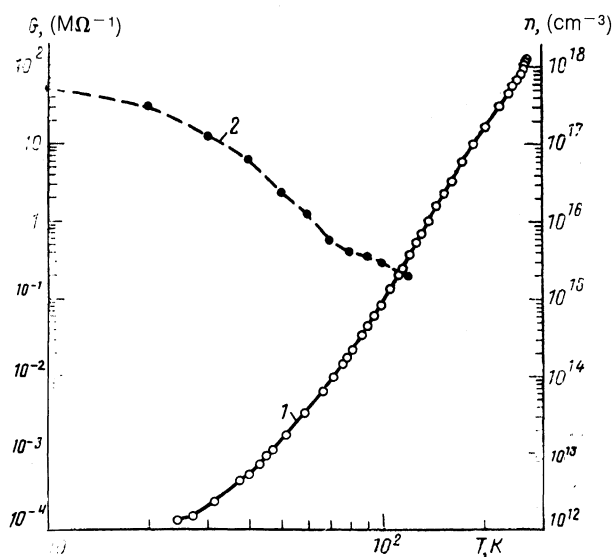


FIG. 2. Conductivity  $G$  of sample No. 2 vs the temperature  $T$ . 1—Cooling in darkness (dark conductivity  $G_d$ ), 2—values of  $G_i$  after illumination for 20 min. Right-hand ordinate scale—result of recalculation using the Drude formula for  $l = 1 \text{ \AA}$ .

PbTe:O films. We assume therefore that the variations of the random potential for the carriers in PbTe:O films exceed the band gap  $E_g \approx 0.2 \text{ eV}$ .

All the films were under normal atmospheric conditions after preparation, i.e., oxidized to saturation. Small changes of the impurity distributions at  $T = 300 \text{ K}$  lasted an indefinitely long time. During a measurement cycle the sample was therefore kept in liquid nitrogen in the intervals between the experiments.

The film conductivity was measured by the simplest two-contact method. Gold or platinum contacts of  $\sim 1 \text{ cm}^2$  area, and hence of minimum resistance, were used. The mea-

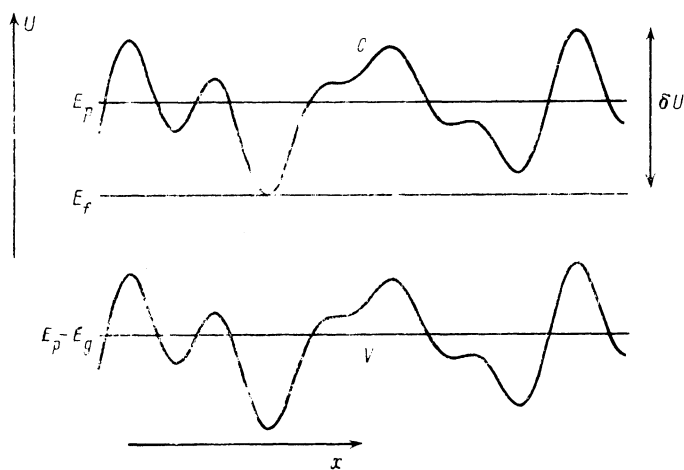


FIG. 3. Schematic representation of the electron potential energy  $U$  in the conduction band  $C$  in the valence band  $V$  vs the coordinate  $x$ ;  $E_p$ —percolation level (mobility threshold),  $E_f$ —Fermi level,  $\delta U$ —characteristic fluctuations of the energy  $U$ .

sured films had a width  $b = 5$  mm and a length  $L = 0.5$  mm, so that the relation between the conductivity  $G = g(bd/L)$  and the electric conductivity  $g$  was  $G = 10gd$ . Voltage was applied to the film by a voltage source  $\mathcal{E} = 1.6$  V. The value of  $G$  was independent of  $\mathcal{E}$  up to  $\mathcal{E} = 10$  V. The measured current values were fed to a computer and recorded on a magnetic disk. The resistance-registration time constant was  $\sim 0.1$  s. Very high resistances were measured in individual experiments with a high-resistance electrometer or, to increase the speed, with a digital oscillograph.

The specimen was surrounded by an opaque screen and illuminated through a glass window by a laser of wavelength  $\lambda = 0.63 \mu\text{m}$ . The holder with the sample were cooled, together with the screen and an optical window, to a low temperature. The large absorption by the glass at  $\lambda > 3 \mu\text{m}$  ensured a lower background due to thermal radiation at room temperature. The light intensity corresponded to a photon flux  $I_m = 10^{15} \text{ cm}^{-2} \cdot \text{s}^{-1}$  on the sample surface. Figure 2 shows the measured dark conductivity of one of the specimens. The use of a relatively low-resistance instrument in these experiments set a lower limit  $G \gtrsim 10^{-4} \text{ M}\Omega$  on the measured conductivity. In the random potential relief schematically illustrated in Fig. 3 one can distinguish two energy levels: a Fermi level  $E_f$  and a percolation level  $E_p$ , also called the mobility threshold. It can be assumed<sup>17</sup> that the temperature dependence of the conductivity defined as  $G(T) = G_0 \cdot \exp[(E_f - E_p)/k_B T]$ .

From the data of Fig. 2 we obtain  $E_p - E_f = 0.12$  eV at  $T = 270$  K and  $E_p - E_f = 0.063$  eV at  $T = 100$  K, i.e., when the temperature is lowered the variations  $\delta U$  decrease together with the band gap  $E_g$ . Following Mott, we assume the minimum carrier mean free path to be  $l \approx 0.1a = 10^{-8}$  cm. The maximum possible density  $n_m$  of the free carriers having energies higher than  $E_p$  can therefore be estimated from the Drude formula  $g = ne^2 l / p$ , where the carrier momentum at room temperature is  $p = (3m^* k_B T)^{1/2} = 2.5 \cdot 10^{-21}$  g·cm/s. From the value  $G = 100 \text{ M}\Omega^{-1}$  we get the estimate  $n_m = 1 \cdot 10^{18} \text{ cm}^{-3}$ . At this density we would have in the homogeneous case a Fermi temperature  $T_f \approx 800$  K, i.e., the electron gas would be degenerate already at room temperature. Interestingly, at this value of  $n_m$  the Debye radius is  $r_D = 300 \text{ \AA}$  for both a degenerate and a nondegenerate electron gas at room temperature. The value of  $r_D$  is strikingly close to the characteristic value of the transverse dimension of the  $p$ -regions seen on Fig. 1a.

Alloying fluctuations led to poor reproducibility of the  $G(T)$  dependences for different specimens prepared under identical conditions. The  $G(300 \text{ K})$  values could differ by 2–3 times, while the  $G(4.2 \text{ K})$  diverged by two orders. If, however, the sputtering rate was changed, the  $G(T)$  spread increased even more. The situation was aggravated by the noticeable difference between the noticeable difference between the thermal expansion coefficients of glass and PbTe, which caused the films to be in a stressed state. Successive cooling of one and the same specimen therefore caused  $G(4.2 \text{ K})$  spread up to 50%. Only multiple thermal cycling stabilized the values of  $G(T)$ . Nonetheless, in a certain set of measurements we tried not to raise the specimen temperature above 150 K. Strictly speaking, the random potential realized was different after each heating of the specimen to room temperature.

## PRIMARY AND SECONDARY ILLUMINATIONS

Typical growth curves of the conductivity with increase of the illumination time  $t$  are shown in Fig. 4. We shall designate as primary the illumination of a specimen cooled in darkness. Turning the light off was followed by a decrease of  $G$ , which can naturally be called relaxation. In the experiments described we used extensively repeated exposures to the light, which we call secondary illumination. As seen from Fig. 4, the secondary illumination differs radically from the primary.

We introduce the following notation:  $t_1$  is the instant when the light is turned on,  $G_1 = G(t_1)$ ,  $t_2$  is the instant of the second illumination, and  $G_2 = G(t_2)$ . The interval from  $G_2$  to  $G_1$  in the course of the secondary illumination was 1.5 s, as against  $\sim 1000$  s for the first illumination. Characteristically, within  $< 0.1\%$ , we have not only  $G(t_2 + 1.5 \text{ s}) = G_1$  but also  $\dot{G}(t = t_2 + 1.5 \text{ s}) = \dot{G}(t = t_1 - 1 \text{ s})$ . Figure 5 shows the initial sections of the three processes, with the time origin of the primary illumination coincident with  $t_1$  and  $t_2$ . In addition, for the relaxation and the secondary illumination the ordinate is measured from the value of  $G_2$ . The maximum of  $\dot{G}(t)$  for the primary illumination was reached at  $t \gtrsim 1$  s and amounted to  $\dot{G}_{m1} \approx 0.56 (\text{M}\Omega \cdot \text{s})^{-1}$ . For the secondary illumination, the first point at  $t = t_2 + 0.09$  s corresponds to a voltage  $U$  integrated over the preceding  $\sim 0.1$  s time interval, i.e., the ratio  $G(t_2 + 0.09 \text{ s})/0.09$  s yields a certain value  $\dot{G}(t \rightarrow t_2) = 100 (\text{M}\Omega \cdot \text{s})^{-1}$  averaged over the indicated interval. We shall arbitrarily call this value the maximum derivative for the secondary illumination and designate it by  $\dot{G}_{m2}$ . Measurements with a digital oscillograph have shown that when  $t = t_2$  is approached  $\dot{G}$  increases up to  $\Delta t \sim 1$  ms. We have subsequently confined ourselves, however, to the study of processes having a time constant  $\sim 0.1$  s, in view of the low accuracy of the oscillograph. Even the averaged  $\dot{G}_{m2}$  exceeds  $\dot{G}_{m1}$  by more than two orders.

Multiple repetition of the relaxation–secondary illumination cycle, i.e., turning the light on and off repeatedly at

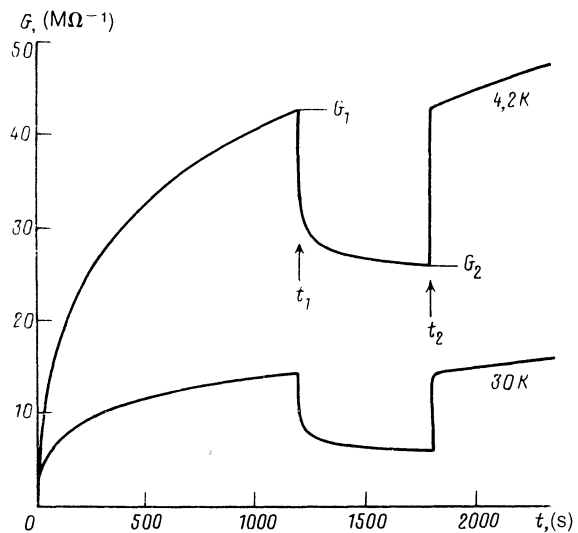


FIG. 4. Conductivity  $G$  of sample No. 2 vs the time  $t$ . Interval  $0 \leq t < t_1$ —primary illumination,  $t_1 \leq t < t_2$ —relaxation in darkness,  $t_2 \leq t$ —secondary illumination.

$T = 4.2$  K, yields identical curves. Only the values of  $G_1$  increase with increase of the total specimen exposure time. On the other hand,  $G_2$  decreases with increase of the relaxation duration  $t_R = t_2 - t_1$ . To compare the secondary-illumination curves obtained in experiments with alternation of the processes for different times  $t_R$ , we normalized the conductivity relative to  $G_1 - G_2$ . Figure 6 shows results of the influence of the relaxation duration on the secondary-illumination process. Note that the changes of the curves with increase of  $t_R$  do not reduce to changes of the abscissa and ordinate scales. The initial illumination rate is the same for all curves, while the "long tail" to reach the initial value of  $G_1$  rises noticeably with increase of  $t_R$ .

Summarizing the analysis of many curves, examples of which are shown in Figs. 5 and 6, we can conclude that the relaxation observed at  $T = 4.2$  K is not a return of the specimen to the initial dark state. We use next the term "primary centers" for the initial deep states at thermal resonance with the crystal. The specimen cooled in darkness was actually in thermal equilibrium, since the  $G_d(t)$  curves and the  $G(t)$  curves obtained after exposure to light were independent, in a wide range, of the cooling rate. Illumination produces free carriers, and the deep centers go over into a new metastable state. We shall designate this state as "secondary centers." The return of the secondary centers to the initial primary state will be called recombination. It can thus be stated that the FPC relaxation at  $T = 4.2$  K is not recombination of secondary centers. But the conductivity decrease undoubtedly constitutes electron localization in a random potential relief. This can be represented as capture of free carriers by traps. The role of these traps can be played also by secondary centers. This has little bearing on the statement that after a time  $t_R \sim 10^5$  s at least 90% of the secondary centers fail to return to the initial primary state.

The situation changes when the temperature is raised.

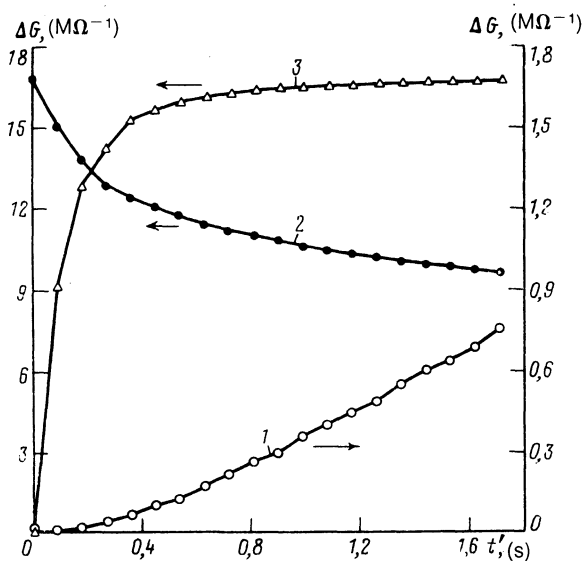


FIG. 5. Initial sections of the three processes shown in Fig. 4: 1—primary illumination,  $t' = t$ ; 2—relaxation,  $t' = t - t_1$ ,  $\Delta G = G - G_2$ ; 3—secondary illumination,  $t' = t - t_2$ .

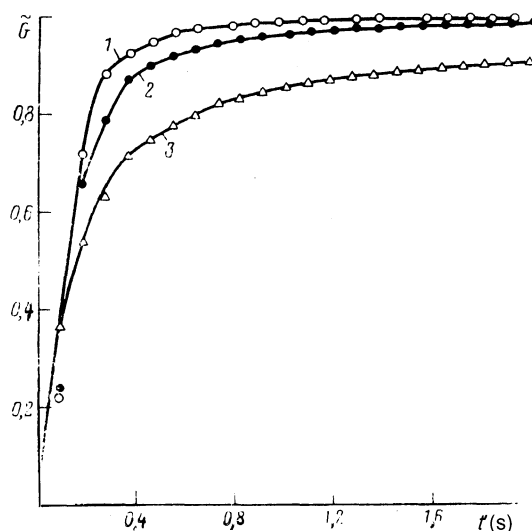


FIG. 6. Plots of secondary illumination after relaxation with various durations  $t_R$ : 1— $t_R = 5$  min, 2—4 h, 3—64 h. Specimen No. 2.  $T = 4.2$  K,  $\tilde{G} = (G - G_2)/(G_1 - G_2)$ ,  $t' = t - t_2$ .

We have repeatedly switched the light on and off a number of times at  $T = 77$  K, increasing  $t_R$  to seven days ( $6 \cdot 10^5$  s). Examples of these secondary-illumination curves are shown in Fig. 7. It is clear both from the value of  $\tilde{G}_{m2}$  and from the ratio  $G(t_2 + t_s)/\Delta G$ , where the time  $t_s$  corresponds to the condition  $\dot{G}(t = t_2 + t_s) = \dot{G}_{m1}$ , that about one-half of the secondary centers could recombine after an interval  $t_R \sim 10^5$  s. A more definite analysis is difficult, as will be made clear below, by the large number of factors. It is seen from Fig. 7, in particular, that recombination of the secondary centers cannot be described as  $\exp(-t/\tau)$  with a certain constant  $\tau$ .

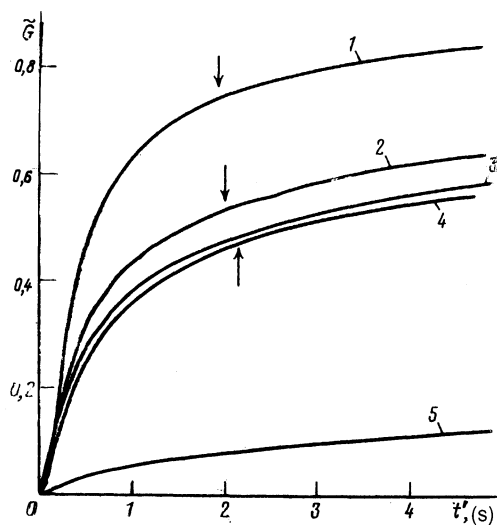


FIG. 7. Secondary-illumination curves after relaxation with various durations  $t_R$ : 1— $t_R = 5$  min, 2— $t_R = 20$  min, 3— $t_R = 3$  day, 4— $t_R = 7$  day. Sample No. 3,  $T = 77$  K. Curve 5—primary illumination  $t' = t$ . Normalization by using the values of  $G_1$  and  $G_2$  from curve 1;  $\tilde{G} = (G - G_2)/(G_1 - G_2)$ ,  $t' = t - t_2$ . The arrow shows the instant of time  $t_s$  at which the slope of the secondary-illumination curve is equal to the average slope of the primary at  $t = 0.5$  s.

## PHOTOEXCITED ELECTRONS

Light-emitting diodes were used in individual experiments to measure the light-absorption coefficient  $\kappa$  defined by the relation  $I = I_0 \exp(-\kappa d)$  for the intensity  $I$  of the light passing through a PbTe film of thickness  $d$ . According to Ref. 18,  $\kappa = 7.0 \cdot 10^5 \text{ cm}^{-1}$  at  $\lambda = 0.63 \mu\text{m}$ , which agrees with our measurement results. The value of  $I/I_0$  remains unchanged, accurate to  $\sim 10\%$ , both after cooling to 4.2 K and with increase of the photoconductivity when the light is turned on after cooling the sample in darkness. This result was expected beforehand, since  $\kappa$  is determined by valence electrons whose density is much higher than that of the photosensitive centers.

Since  $\kappa$  is large, light is weakened by more than 1000 times in films with  $d \approx 1000 \text{ \AA}$ . A tenfold lowering of the intensity was observed even in thin films with  $d \approx 300 \text{ \AA}$ . To explain the consequences of so inhomogeneous an illumination, experiments were performed in which the primary illumination was applied to one side of the film, and after relaxation in darkness the specimen was rotated and the secondary illumination was applied to the other side. Note that in the usual organization of the experiments the light from the source was likewise incident only on one side of the film after passing through the optical window. Numerous reflections from the film, the substrate, and the walls of the copper screen, however, ensured illumination of both sides of the film. In experiments with unilateral illumination the screen was made of black mat photographic paper, the reflection from which could be neglected.

In experiments with alternating unilateral illumination one could expect the characteristic differences of the secondary illumination to vanish, in view of the poor optical transmission of the PbTe film, so that for the dark side the repeated illumination was in fact the primary one. Figure 8 shows plots that refute these expectations. Experiments with alternate-side illumination have shown that in a film  $< 700 \text{ \AA}$  thick approximately the same number of secondary centers appear on the dark side as in the case of unilateral illumination, when  $G(t_2 + 1.5 \text{ s}) = G_1$  accurate to  $\approx 0.1\%$ . It can be assumed that an energetic photon with  $\hbar\omega \approx 2 \text{ eV}$  excites one of a set of valence electrons near the illuminated side of the sample. The excited electron gives up relatively rapidly, in a time  $10^{-14} - 10^{-15} \text{ s}$ , the greater part of its energy to the surrounding valence electrons, the number of which is of the order of  $\hbar\omega/k_B \Theta \sim 10^2$ . Next, each excited electron is thermalized much more slowly on account of photo emission. Ultimately the excited electrons can reach the opposite surface of the specimen and ionize primary centers. Electron excitation of freezing-in centers was observed<sup>15</sup> following injection, with the aid of the tunnel effect, of electrons of energy  $\sim 1 \text{ eV}$  into a PbTe:O film.

Comparison of the two curves of Fig. 8, corresponding to different alternations of the illuminated sides, points to a noticeable difference between the relaxation near a free film surface bordering on liquid helium and in the strongly stressed part of the film near glass. During the primary illumination the two curves differ insignificantly. The relaxation proceeds more rapidly, however, if the boundary with glass is illuminated. More filled traps are produced there, since  $G(t_2 + 1.5 \text{ s}) > G_1$  for the secondary illumination from the glass side. In the opposite sequence, on the contrary,  $G(t_2 + 1.5 \text{ s}) < G_1$ . This difference becomes even more

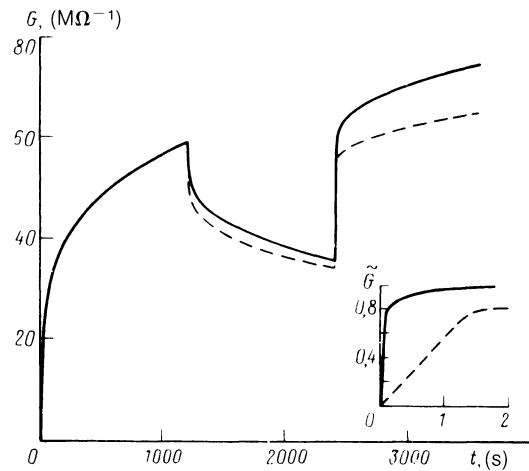


FIG. 8. Photoconductivity curves obtained for primary and secondary illumination from opposite sides of the target. Solid curve—primary illumination from the free-surface side, secondary—from the glass-substrate side; dashed—primary from the substrate side, secondary from the helium side. Inset—comparison of relative changes of  $\tilde{G}$  as function of  $t'$  and start of primary illumination. Sample thickness  $d = 690 \text{ \AA}$ ,  $T = 4.2 \text{ K}$ .

impressive when the film thickness is increased. For example, at  $d = 1000 \text{ \AA}$  we have for secondary illumination from the glass side  $G(t_2 + 1.5 \text{ s}) - G_1 \approx G_1 - G_2$ , but on the contrary  $G_1 - G(t_2 + 1.5 \text{ s}) \approx (G_1 - G_2)/2$  for secondary illumination from the helium side. At larger film thickness, the excitation energy of the electrons diffusing through the film is on the average decreased. We must conclude thus that traps near the free and stressed surfaces capture free carriers in different manners and have different ionization potentials.

## MODEL OF FROZEN-IN PHOTOCONDUCTIVITY

As indicated above, we can assume for the electrons in oxidated PbTe films a random-potential variation  $\delta U \lesssim E_g$ . Let us estimate the probability  $P$  of carrier tunneling in PbTe under a rectangular barrier of height  $\delta U = 0.2 \text{ eV}$  and of width  $x = 150 \text{ \AA}$ . From the known equation  $P = \exp[-2(2m^*\delta U)^{1/2} x/\hbar]$  we obtain  $P \sim 10^{-7}$ . We assume a cross section  $\sigma = 10^{-16} \text{ cm}^2$ , for recombination of a secondary center with one of the free electrons, and for the free electron  $a$  density  $n = 10^{18} \text{ cm}^{-3}$  and a velocity  $v = 5 \cdot 10^7 \text{ cm/s}$ . The recombination time for a photoionized center located in the below-barrier region is then  $\tau_r = (Pnv\sigma)^{-1} \lesssim 10^{-2} \text{ s}$ . Errors of one or two orders of magnitude cannot change the main conclusion that owing to the tunnel effect the recombination time  $\tau_r$  for our specimens cannot exceed noticeably 1 s. Regardless of the process producing the secondary centers, in the simplest representations carrier localization on the center is a transition of the system to a ground state lower than all others. Tunneling ensures that this state can be reached in a time  $\tau_r < 1 \text{ s}$ . We emphasize that we are not dealing here with relaxation, which is essentially characterized at the start of the process by times  $\sim 10^{-2} \text{ s}$ . By true frozen-in photoconductivity we mean here the fact that the number of secondary centers is not noticeably decreased, say by 10%, in a time  $\sim 3 \cdot 10^5 \text{ s}$ .

We assume that the barriers hindering the return of the secondary centers to the ground state are undoubtedly due to deformation of the crystal lattice. In view of the large ion masses, tunneling does not play a noticeable role here. On the contrary, as seen from Fig. 2, raising the lattice temperature to  $T \approx \Theta$  eliminates the frozen-in superconductivity.

Following Volkov and Pankratov,<sup>7,9</sup> we introduce a perturbation potential  $V(r)$  corresponding to deviations from the potential of an ideal crystal due to the presence of a point defect at a crystal-lattice site of a  $A^4B^6$  compound. The spectrum of the electrons localized on the defect is determined by the value of  $V(r)$ . We denote by  $\varphi_\beta(r)$   $p$ -orbitals with indices  $\beta = x, y, z$ , centered at the site  $r$ . If only the diagonal element  $g_- = \langle \varphi_\beta(r) | V(r) | \varphi_\beta(r) \rangle$ , is taken into account for a short-range perturbation potential, bound states of energy  $E_0^* \sim E_g$  will be produced in the defect on site A only for  $g_- < 0$ , i.e., for attraction of electrons to the center, and on a defect in site B only for  $g_- > 0$ , i.e., for repulsion.<sup>7,9</sup> The subscript of  $g$  indicates that the states produced pertain to an odd representation, namely  $\Gamma_{15}^-$ . When the nearest-neighbor overlap integrals are taken into account, we must introduce  $g_\pm = \langle \varphi_\beta(r \pm a) | V(r) | \varphi_\beta(r \pm a) \rangle$ .

The solutions pertain now to a reducible even representation  $\Lambda^+$ , appearing on the site A at  $g_+ > 0$  and at site B at  $g_+ < 0$ . In all cases,  $g_\pm > 0$  means separation of a state from the valence band and its upward motion with increase of the perturbation. For  $g_\pm < 0$ , on the contrary, the local state is separated from the conduction band and drops lower the stronger the perturbation. As noted in Refs. 7 and 9,  $V(r) > 0$  for Pb or Te vacancies. We assume that in the oxygen-impurity case of interest to us we should put  $V(r) < 0$  since the oxygen atoms are highly electronegative. For substitution impurities we can use the results of Refs. 7 and 9 and assume that an oxygen atom at the location of a lead atom produces local levels  $E_0^*$  that can lie deeply in the valence band; when the tellurium is replaced by oxygen,  $E_0^*$  levels can be produced near the bottom of the conduction band  $E_c$ ; hybridization of the states may result in  $E_0^* > E_c$ . The spectrum of the interstitial locations of the O atoms calls for a special analysis, although the possibility of onset of a local state is obvious. Starting from general considerations concerning valence bonds, we assume that the ground state of the  $O^{2-}$  impurity corresponds to two electrons localized on a deep center. The O atom binds two electrons from those supplied by the donors to the conduction band. Oxygen serves therefore as a compensating impurity for  $n$ -PbTe crystals.

As verified in detail in Ref. 19, frozen-in photoconductivity is due to lattice deformation near a defect whose charge state has been altered. We denote by  $\nu$  the number of electrons filling the  $E_0^*$  level, and by  $q_i$  the normal coordinates describing the displacements of atoms from equilibrium positions at  $\nu = 0$ . We expand the electron Hamiltonian in powers of  $q_i$ :

$$\hat{\mathcal{H}} = \hat{\mathcal{H}}_0 + \sum_i \frac{\partial \hat{\mathcal{H}}}{\partial q_i} q_i + \sum_i \frac{\partial^2 \hat{\mathcal{H}}}{\partial q_i^2} \frac{q_i^2}{2}. \quad (1)$$

In first-order perturbation theory, the sum of the energy of

an electron term of a localized state and the elastic lattice-deformation energy is

$$E_i = E_0^* + \sum_i (W_i q_i + K_i q_i^2 / 2), \quad (2)$$

where the matrix elements  $W_i = \langle 0 | (\sigma \hat{\mathcal{H}} / \partial q_i) | 0 \rangle$  are determined by the unperturbed functions of the state  $E_0^*$ , and the elastic coefficients  $K_i$  are constants. At  $\nu = 0$  all  $W_i \approx 0$  by virtue of the local character of the perturbation potential. For  $\nu \neq 0$  most  $W_i = 0$  by virtue of the symmetry of the problem. We discuss hereafter for simplicity the case  $\nu = 1$ , since the change to  $\nu = 2$  can be effected by doubling the energies and taking the  $e$ - $e$  interaction energy into account.

Since our purpose is illustration, we shall not expand the total vibrational representation into irreducible ones, and attempt to estimate the coefficients  $W_i$  and  $K_i$ . We retain in Eq. (2) only terms with  $q_1$ , and set the others equal to zero. We introduce a bias  $Q_1 = -W_1 K_1$ , and rewrite (2) in the form

$$E_i = E_0^* + K_1 (q_1 - Q_1)^2 / 2 - K_1 Q_1^2 / 2. \quad (3)$$

The delocalized-electron term is  $E_0 = K_1 q_1^2 / 2$  if the bottom of the conduction band is chosen as the origin. The term crossing  $E_0 = E_1$  that occurs in the adiabatic approximation determines the crossing-point abscissa  $q_1 = \tilde{q} = E_0^* / K_1 Q_1$ . The term crossing for the case  $K_1 Q_1^2 \geq E_0^*$ , when the point  $\tilde{q}$  lies between extrema of  $E_0$  and  $E_1$ , is shown in Fig. 9. We assume that the filled state  $E_1$  corresponds to the primary center, so that the minimum of the parabola  $E_1$  lies lower than  $E_f < E_c$ . The delocalized state  $E_0$ , on the contrary, corresponds to a secondary state of the center and to the presence of a free carrier. The illumination is denoted by a vertical arrow from  $E_1$  to  $E_0$ , parallel to the ordinate axis in accordance with the Franck-Condon principle. The return of the center to the primary state denotes a nonradiative  $E_0 \rightarrow E_1$  transition with surmounting of a barrier  $\tilde{U}$ . In other words, recombination of the secondary centers after illumination can be due only to vibrations of a lattice with the activation energy

$$\tilde{U} = \frac{(E_0^* - K_1 Q_1^2)^2}{2K_1 Q_1^2}. \quad (4)$$

The temperature dependence of the recombination time for frozen-in photoconductivity is given approximately by

$$\tau_r = \tau_e \exp \left\{ \frac{2\tilde{U}}{\hbar\omega_1} \operatorname{th} \left( \frac{\hbar\omega_1}{2k_B T} \right) \right\}, \quad (5)$$

where  $\tau_e = \text{const} \sim 10^{-8}$  s is of the order of the electronic transition times, and  $\hbar\omega_1$  denotes the quantum energy of the normal oscillations  $q_1$ . For a real case, when the vibronic coupling coefficients  $W_i$  are not zero for several oscillation modes, Eq. (5) becomes quite unwieldy.<sup>9</sup> We confine ourselves to an estimate in which  $q_1$  is taken to be the transverse optical mode  $\omega_{\text{TO}}$ . According to the neutron-diffraction data of Ref. 20 for PbTe,  $\hbar\omega_{\text{LO}} = 160$  K and  $\hbar\omega_{\text{TO}} = 50$  K. It appears that owing to the symmetry of the problem, the LO mode is not very effective and the TO mode yields  $\tau_r \sim 10^8$ - $10^9$  s for  $\tilde{U} \sim 0.1$  eV in the temperature region

$T \lesssim 25$  K, when we can assume that  $\text{th}(\hbar\omega_1/2k_B T) \approx 1$  in (5). On the contrary, for  $T \gtrsim 50$  K we can write in lieu of (5)

$$\tau_i \approx \tau_e \exp(\bar{U}/k_B T). \quad (6)$$

This shows the strong decrease of  $\tau$ , when the temperature is raised. For  $T \approx 0.1 \bar{U}/k_B \approx 100$  K we obtain  $\tau_i \sim 10^{-4}$  s, meaning that the frozen-in superconductivity vanishes. Note that we must write  $\tau_r$  in place of  $\tau_e$  for the below-barrier center considered by us at the beginning of the section.

If a weaker vibronic coupling  $K_1/Q_1^2 < E_0^*$  is assumed, so that  $\bar{q} > Q_1$  and the intersection of the parabolas lies, unlike in Fig. 9, to the right of the minimum of  $E_1$ , the transition  $E_0 \rightarrow E_1$  can take place at constant  $q_1$  on account of emission of a photon. Estimates of the radiative-transition probabilities are known (see, e.g., Ref. 21). Under the most favorable premises can a value  $\tau_i > 1$  s be obtained in this case. Thus, the large value  $\tau_i > 10^6$  s observed in experiment denotes a strong vibronic interaction for a deep center for an oxygen impurity.

### KINETICS OF ILLUMINATION AND RELAXATION

We derive now simple phenomenological relations. We assume for the sake of argument that the primary centers are negatively charged acceptors produced by an oxygen admixture with density  $n_0$ . The number of free carriers—electrons with density  $n = n(t)$ —is increased by illumination through photodissociations of  $O^{2-}$  acceptors that are transformed into metastable secondary centers. We denote by  $\sigma_1$  the cross section of this process, and by  $n_1 = n_1(t)$  the density of the primary centers. The free, meaning delocalized, nonequilibrium carriers become localized with growing thermalization—in other words, they are captured in traps. The traps can be either secondary centers or other defects. Generally speaking we observe an Anderson localization of the nonequilibrium carriers in a random potential. Independently of

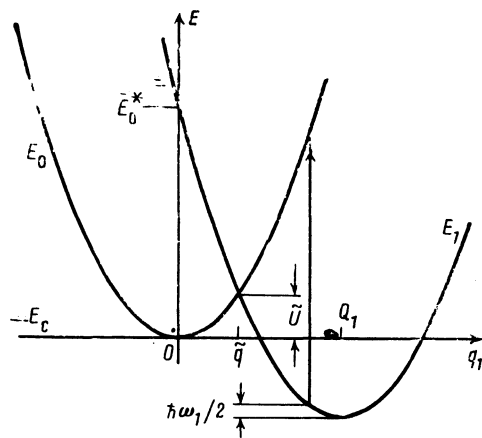


FIG. 9. Electron energy plus elastic lattice-deformation energy corresponding to the normal coordinate  $q_1$ ;  $E_0$ —delocalized electron on the bottom of the conduction band  $E_c$ ,  $E_1$ —electron localized on a deep center,  $E_0^* = E_1(q_1 = 0)$ ,  $Q_1$  equilibrium position for a filled deep center,  $\bar{q}$ —abscissa of term crossing,  $\bar{U}$ —localization energy barrier,  $\hbar\omega_1$ —quantum of normal oscillation  $q_1$ .

the mechanism that localizes the excited carriers, we characterize this process by a time  $\tau = \text{const}$ . The localized carriers can again become free by the action of light or by electron impact. We do not know the charge state of the traps, and will refer for simplicity to ionization of traps characterized by a cross section  $\sigma_2$ . It follows from experiment that  $\sigma_2 \gg \sigma_1$ . We shall consider only the case of sufficiently low temperature, when recombination of secondary centers can be neglected. We introduce the following notation:  $I$  ( $\text{cm}^{-2} \cdot \text{s}^{-1}$ ) is the photon flux density,  $\omega_1 = I\sigma_1$ ,  $\omega_2 = I\sigma_2$ , and  $\omega_3 = I\sigma_2 + \tau^{-1}$ . The kinetic equations are

$$\dot{n}_1 = -\omega_1 n_1, \quad \dot{n} = \omega_1 n_1 + \omega_2 (n_0 - n_1 - n) - n/\tau. \quad (7)$$

Under the initial conditions  $n_1(0) = n_0$  and  $n(0) = 0$  Eqs. (7) have a solution  $n_1 = n_0 \exp(-\omega_1 t)$  and

$$\frac{n}{n_0} = \frac{\omega_2}{\omega_3} (1 - e^{-\omega_3 t}) - \frac{\omega_2 - \omega_1}{\omega_3 - \omega_1} (e^{-\omega_1 t} - e^{-\omega_3 t}). \quad (8)$$

Analysis of the experimental results has shown that distributions in  $\sigma_1$  must be introduced for the primary centers in  $\sigma_2$  and  $\tau$  for traps. We designate the lower and upper limits of the intervals by  $\sigma'_1 \leq \sigma_1 \leq \sigma''_1$ ,  $\sigma'_2 \leq \sigma_2 \leq \sigma''_2$ , and  $\tau_1 \leq \tau \leq \tau_2$ . We introduce the parameters  $s_1 = \ln(\sigma''_1/\sigma'_1)$ ,  $s_2 = \ln(\sigma''_2/\sigma'_2)$ , and  $q = \ln(\tau_2/\tau_1)$ . Note that the expected values are  $s_2 \gtrsim 2$ ,  $s_1 \gtrsim 5$  and  $q \gtrsim 10$ . With an aim at obtaining agreement with experiment, we specify distribution functions defined by the relations

$$\frac{dn_1}{d\sigma_1} = \frac{n_0}{s_1} \frac{1}{\sigma_1}, \quad \frac{dn_2}{d\sigma_2} = \frac{n_2}{s_2} \frac{1}{\sigma_2}, \quad \frac{dn}{d\tau} = \frac{n}{q} \frac{1}{\tau}. \quad (9)$$

To write down the results we shall need the integral exponential function  $E_1(z)$  defined as

$$E_1(z) = \int_z^\infty \frac{e^{-\xi}}{\xi} d\xi$$

for  $|\arg z| < \pi$  (Ref. 22). A valid expansion at  $z \ll 1$  is

$$E_1(z) \approx -\gamma - \ln z + z,$$

where  $\gamma = 0.5772$ . For  $z \gg 1$  we can use the asymptotic approximation  $E_1(z) \approx \exp(-z)/z$ . For simplicity we introduce a special function  $F(z) \equiv \gamma + \ln z + E_1(z)$ , given by  $F(z) \approx z$  for  $z \ll 1$  and  $F(z) \approx \ln z$  for  $\ln z \gg 1$ . We put  $w'_1 = I\sigma'_1$  and  $w''_1 = I\sigma''_1$ . After integrating (8) over the distribution of  $\sigma_1$  we obtain at  $w'_1 t \ll 1$

$$\begin{aligned} \frac{n}{n_0} s_1 &= \frac{w_2 \tau}{w_2 \tau + 1} F(w'_1 t) \\ &+ \frac{\tau/t}{(w_2 \tau + 1)^2} [1 - \exp(-w''_1 t) - w''_1 t \exp(-w_3 t)]. \end{aligned} \quad (10)$$

Integration of (10) over the  $\tau$  distribution yields at  $(I\sigma''_1)^{-1} \ll t \ll (I\sigma'_1)^{-1}$  an expression for the primary illumination:

$$n = \left[ 1 - q^{-1} \ln \left( 1 + \frac{1}{I\sigma_2 \tau_1} \right) \right] \bar{n}_0(t), \quad (11)$$

where

$$\tilde{n}_0(t) = (n_0/s_1)F(I\sigma_1''t). \quad (12)$$

The logarithmic time dependence  $F \approx \ln t$  predicted by Eq. (12) for  $I\sigma_1''t \gg 1$  was observed for hundreds of experimental curves with characteristic value  $(I\sigma_1'')^{-1} \approx 30$  s at  $T = 4.2$  K, corresponding to  $\sigma_1' \approx 0.3 \cdot 10^{-16}$  cm<sup>2</sup>. The illumination curves did not reach saturation even for  $t \approx 3 \cdot 10^4$  s. The ratio  $\sigma_1''/\sigma_1'$  exceeded thus three orders of magnitude and we have obtained only the upper bound estimate  $\sigma_1' < 10^{-20}$  cm<sup>2</sup>.

The initial steep section of the primary illumination is not described by Eq. (12). We had to introduce empirically in (12) a supplementary term leading to

$$\tilde{n}_0(t) = (n_0/s_1) [F(w_1''t) + C_1(1 - \exp(-C_2w_1''t))]. \quad (13)$$

The fit parameters were  $n_0/s_1$ ,  $w_1'' = I\sigma_1''$ ,  $C_1$ , and  $C_2$ . With a computer and successive approximations it was possible to choose the parameters quite rapidly. The result of such a fit for one of the numerous primary-illumination curves is shown in Fig. 10. The deviations of the experimental data from Eq. (13) are represented by the deviations of the dashed curve from the straight line joining the origin with the end of the continuous curve. Evidently, Eq. (13) really describes the results quite well for variation of  $t$  over four orders of magnitude.

The term  $1 - \exp(-C_2w_1''t)$  denotes introduction of one more group of primary centers with definite photoionization cross sections having the same value  $\sigma_1 = C_2\sigma_1''$  for the entire group. The number  $n_0'$  of such centers, referred to the total number  $n_0$ , is  $C_1/s_1$ . The existence of this additional group fits the overall picture of the primary-illumination mechanism.

As already noted, the primary centers become deionized by photon absorption and by impacts of photon-excited electrons. We assume that a wide distribution of the cross sections  $\sigma_1$  in the interval  $\sigma_1' \ll \sigma_1''$  is due precisely to the distribution over the excited electrons in energy  $E$ , since  $\sigma_1$  should obviously depend on  $E$ . An additional group with definite value  $\sigma_1 = C_2\sigma_1''$  corresponds to direct photo-deionization by light near the specimen surface. The change of the intensity  $I$  in the interior of the specimen, which should effectively broaden the  $\sigma_1$  distribution, is already masked by the already present very wide distribution of the centers over the illumination cross section.

As to the distribution in  $\tau$ , it is caused by the already discussed below-barrier tunneling. If the unfilled traps are uniformly distributed over a depth  $x$  below a rectangular barrier of height  $\delta U$ , then for  $q \propto (\delta U)^{1/2}$  we obtain  $\tau = \tau_1 \exp(qx/D)$ , where  $D$  is the upper bound of  $x$ , with  $dn_2 \sim dx \sim d(\ln \tau)$  (Ref. 23).

To verify the theoretical relations we have performed experiments with variation of the incident-light intensity  $I$ . To this end, the laser beam passed through a polarizing Glan prism that could be rotated around the beam axis. The relative change  $I \propto \cos^2 \alpha$  was determined by measuring a rotation angle  $\alpha$ . The angle at which the beam was darkened was defined as  $\alpha = \pi/2$ . Figure 11 shows the secondary illumination processes following application of light of intensity lower than that of the primary. It is clear from Eqs. (11) and (12) that the different value of the stationary level  $G = G_3$  at  $t \gtrsim t_2 = 50$  s is due entirely to the argument of the logarithm

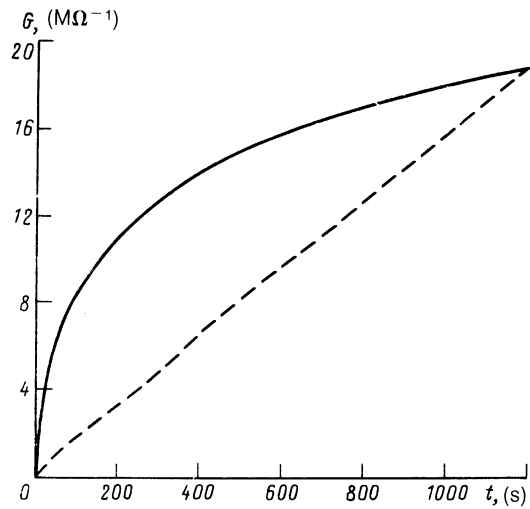


FIG. 10. Comparison of theory with experiment for primary illumination. Solid curve—experimental data; sample No. 1,  $T = 4.2$  K,  $I = I_{\max}$ . The abscissa for the dashed curve is not  $t$  but the quantity  $\xi$  in the square brackets of Eq. (13). The coefficient  $A$  in the relation  $G = A\xi$  is such that the curves coincide at  $t = 1200$  s. The parameter values are  $A = 4.51$  M $\Omega^{-1}$ ,  $w_1'' = 1.46 \cdot 10^{-2}$  s<sup>-1</sup>,  $C_1 = 0.75$ , and  $C_2 = 6.0$ .

in (11) at  $\tilde{n}_0(t_1) = \text{const}$ . It was established in the experiments that  $G_1 - G_3(I) \propto \ln(I_{\max}/I)$ . This agrees with (11) if  $I\sigma_2\tau_1 \ll I$  and makes it possible to determine  $q$ . For example, from the curves of Fig. 11 we obtained  $q = 36$ , which corresponds to  $D \approx 300$  Å according to the equation  $q = 2(2m^*\delta U)^{1/2} D/\hbar$  with  $\delta U = 0.2$  eV.

To describe the relaxation that sets in at the instant  $t = t_1$  we use the notation  $\tilde{n}_{01} = \tilde{n}_0(t_1)$ , where the first part can be determined from Eq. (12) or (13). Integration of the kinetic-equation solution over the distributions of  $\sigma_1$  and  $\tau$  yields

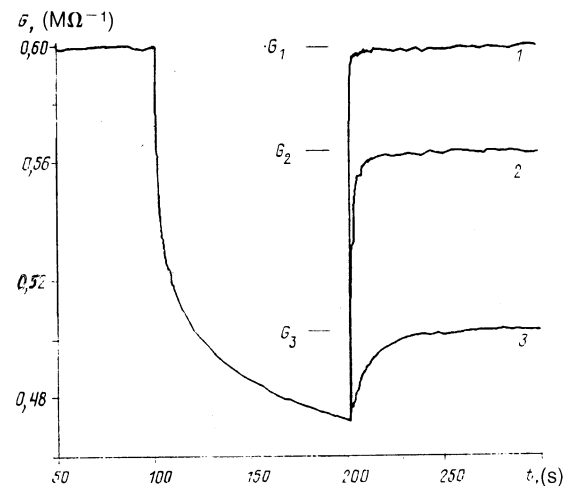


FIG. 11. Relaxation after primary illumination at intensity  $I = I_{\max}$  and secondary illumination at  $I = I_{\max}$  (curve 1),  $I = 0.1 I_{\max}$  (2), and  $I = 0.003 I_{\max}$  (3). Light turned off at  $t_1 = 100$  s and turned on again at  $t_2 = 200$  s. Sample No. 1,  $T = 4.2$  K,  $I_{\max} = 10^{15}$  cm<sup>-2</sup>·s<sup>-1</sup>.

$$\frac{n(t_R)}{\tilde{n}_{01}} = 1 - q^{-1} \left\{ F\left(\frac{t_R}{\tau_1}\right) + \exp(w_2 t_R) \times \left[ E_1(w_2 t_R) - E_1\left(w_2 t_R + \frac{t_R}{\tau_1}\right) \right] \right\}, \quad (14)$$

where the argument  $t_R$  denotes the duration of the relaxation process. At  $t_R \gg (I\sigma_2)^{-1}$  only the first term remains between the curly brackets of (14), using  $n(t_1)$  given by Eq. (11) and the approximation for  $F(t_R/\tau_1)$  at  $t_R \gg \tau_1$ , we get

$$\frac{n(t_R)}{n(t_1)} = \frac{q - \ln(t_R/\tau_1)}{q - \ln\left(1 + \frac{1}{I\sigma_2\tau_1}\right)}. \quad (15)$$

Such is the simple equation for the relaxation "tail." Figure 12 shows the values of  $G$  measured for relaxation from one and the same illumination level  $G_1$ . The level  $G_1 = \text{const}$  was reached at various light intensities  $I$  by suitable variation of the illumination duration  $t_1 \propto I^{-1}$ . The decisive role of just the summary "dose"  $It$  is a characteristic property of frozen-in photoconductivity. As seen from Fig. 12, for  $t_R$  there is actually observed a linear dependence of  $G(t_R)$  on  $\ln t_R$ , which deviates from a straight line with decreasing  $t_R$  in view of the more complicated dependence in Eq. (14). The abscissa intercept  $t_R^*$  of the extrapolation of the linear section on Fig. 12 is given, according to Eq. (15), by

$$t_R^* = \tau_1 + (I\sigma_2)^{-1} \approx (I\sigma_2)^{-1}. \quad (16)$$

The experimental data agree approximately with  $t_R^* \propto I^{-1}$ . By the same token, the start of the relaxation is determined not by  $\tau_1$  but by the secondary-illumination cross section  $\sigma_2 = (It_R^*)^{-1}$ . From Fig. 12 we have thus  $\sigma_2 \approx 10^{-14} \text{ cm}^2$

for sample No. 1 at  $T = 4.2 \text{ K}$ .

Figure 13 shows data on relaxation from a different illumination level  $G_1$  reached at constant  $I$  after a different time  $t_1$ . The ratio of the values of  $G_1$  for the two outermost curves exceeds 10, but influences little the  $G(t_R)$  curves. According to Eq. (15), the straight lines describing the relaxation in the coordinates  $G$  and  $\ln t_R$  should pass through two points: 1)  $G = G_1$ ,  $t_R = t_R^* \approx (I\sigma_2)^{-1}$ ; 2)  $G = 0$ ,  $t_R = t^{**} = \tau_1 e^q$ . The small change of the slopes of the curves of Fig. 13 corresponds to an increase of  $t^{**}$  with increase of  $G_1$  at almost constant  $t^*$ . Assume that this is due the changes of  $q$ . An increase of  $q$  means then an increase of either the height  $\delta U$  or the width  $D$  of the barrier in the relief of the random potential, i.e., of the carrier density, with increase of  $G_1$ . It is known at the same time that potential difference across the  $p$ - $n$  junction decreases upon illumination, whereas the Debye radius and with it the width of the  $p$ - $n$  junction decreases in view of the increase of the carrier density. Allowance for the possible dependence of  $\tau_1$  on  $G_1$  only strengthens this contradiction. When the carrier density increases,  $\tau$  can only decrease in view of the contribution of the two-particle contribution processes, for which  $\dot{n} \propto -n^2$  and  $\tau_{\text{eff}} \propto n^{-1}$ . We found no satisfactory explanation of this contradiction. We have nevertheless determined, by extrapolating the linear section of the relaxation, in terms of the coordinates  $G$  and  $\ln t_R$ , the order of magnitude of  $t^{**} = \tau_1 e^q$ . With the aid of the curves of Fig. 11 we estimated the value of  $q$  and obtained ultimately an estimate of the relaxation time  $\tau_1$ . We obtained  $\tau_1 \approx 10^{-4} \text{ s}$  for sample 1 at  $T = 4.2 \text{ K}$ .

The last step in the present section is integration of the kinetic-equation solutions over the distribution of the cross sections  $\sigma_2' \leq \sigma_2 \leq \sigma_2''$ . For primary illumination, under the condition  $I\sigma_2\tau_1 \ll I$ , we obtain for  $(I\sigma_2')^{-1} \ll (I\sigma_2)^{-1} \ll t \ll (I\sigma_1')^{-1}$

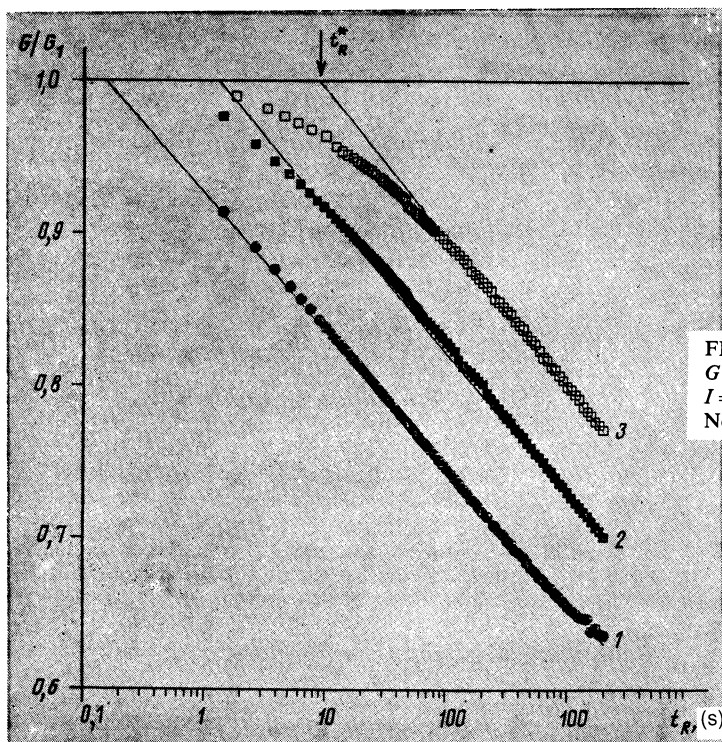


FIG. 12. Relative conductivity in relaxation vs  $t_R = t - t_1$ ,  $G_1 = G(t_1) = \text{const}$ . Primary illumination at various light intensities: 1— $I = I_{\text{max}} = 10^{15} \text{ cm}^{-2} \cdot \text{s}^{-1}$ , 2— $I = 0.1 I_{\text{max}}$ , 3— $I = 0.01 I_{\text{max}}$ . Specimen No. 1,  $T = 4.2 \text{ K}$ .

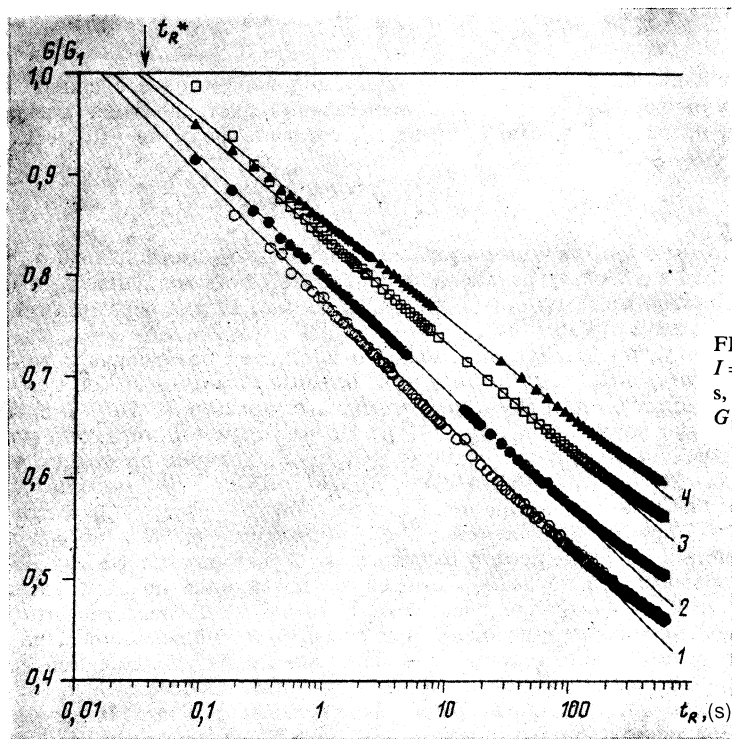


FIG. 13. Photoconductivity relaxation  $G_1$  from various levels reached at  $I = I_{\max}$  at different times  $t_1$ : 1— $t_1 = 30$  s,  $G_1 = 0.41 \text{ M}\Omega^{-1}$ ; 2— $t_1 = 100$  s,  $G_1 = 0.97 \text{ M}\Omega^{-1}$ ; 3— $t_1 = 800$  s,  $G_1 = 2.75 \text{ M}\Omega^{-1}$ ; 4— $t_1 = 4200$  s,  $G_1 = 5.2 \text{ M}\Omega^{-1}$ . Specimen No. 3,  $T = 4.2$  K.

$$n = (n_0/s_1) [1 + q^{-1} \ln(I\bar{\sigma}_2\tau_1)] F(I\sigma_1''t), \quad (17)$$

where the geometric mean of the cross section is  $\bar{\sigma}_2 = (\sigma_2'\sigma_2'')^{1/2}$ . We were unable to obtain for relaxation an analytic solution that covers the entire  $t_R$  interval. A good interpolation formula is

$$\frac{n(t_R)}{n(t_1)} = 1 - \frac{F(\bar{w}_2 t_R)}{\ln(\bar{w}_2 \tau_2)}. \quad (18)$$

where  $w_2 = I\sigma_2$ . Figure 14 shows a comparison of one of the set of experimental curves with Eq. (18). As seen from Fig. 14, the deviations are small. In many experiments at  $T > 20$  K, however, when the relaxation reached  $G/G_1 < 0.5$ , large deviations from (18) were observed. For long times  $t_R$  the slope of  $|\dot{G}|$  was much smaller than predicted by Eq. (18) that describes well the initial relaxation period. In other words, at high  $t_R$  the conductivity  $G$  decreased much more slowly than expected from extrapolation of the initial sections in accord with  $\ln t_R$ . The deviations were particularly strong for sample 3 and prevented data from being obtained for the cross section  $\bar{\sigma}_2$  at intermediate temperatures.

We obtain now the equations for secondary illumination. We use  $t'$  for the duration of the secondary illumination,  $t = t_2$  for its starting instant, and assume that  $n_2 = n(t \leq t_2)$  directly before the start of the illumination. The primary termination is terminated at the instant  $t = t_1$ , and the value of  $\tilde{n}_1 = \tilde{n}_0(t_1)$  is calculated from Eq. (12) or (13). We introduce the notation

$$I\sigma_2' = w_2', \quad I\sigma_2'' = w_2'', \quad v = \tau^{-1}, \quad v_1 = \tau_1^{-1}, \quad v_2 = \tau_2^{-1}.$$

The parameters satisfy the condition  $v_2 \ll w_1 \ll w_2 \ll v_1$ . The solution of the kinetic equation (7) with the specified initial conditions is

$$n(t') = n_2 \exp(-w_3 t') + \tilde{n}_1 (w_2/w_3) [1 - \exp(-w_3 t')]. \quad (19)$$

Integration of (19) over the  $\tau$  distribution yields

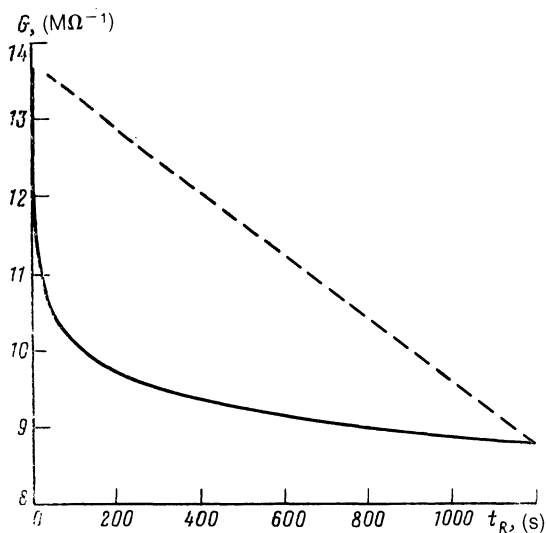


FIG. 14. Comparison of theory with experiment for the relaxation process. Solid curve—experimental data. Sample No. 1,  $T = 10$  K. The abscissa of the dashed curve is not  $t_R$  but, in accordance with (18),  $\xi = F(\bar{w}_2 t_R)/\ln(\bar{w}_2 \tau_2)$ . The coincidence of the initial and final points of the curves was used to determine the proportionality coefficient in the relation  $G = G_1(1 - \xi)$ . The parameters are:  $\bar{w}_2 = 5 \text{ s}^{-1}$ ,  $\tau_2 = e^{23} \text{ s}$ .

$$n(t') = n_2 [1 - q^{-1} F(v_1 t')] \exp(-w_2 t') + \tilde{n}_1 \left\{ 1 - \exp(-w_2 t') + q^{-1} F(v_1 t') \exp(-w_2 t') + q^{-1} \left[ E_1(w_2 t') - E_1(w_2 t' + v_1 t') - \ln \frac{w_2 + v_1}{w_2} \right] \right\}. \quad (20)$$

We were unable to integrate exactly over the  $\sigma_2$  distribution. To estimate the integral of  $E_1$  we used the inequalities satisfied by the parameters under the conditions of our experiments. We obtained ultimately the following interpolation equation:

$$n(t') = \frac{n_2}{s_2} [1 - q^{-1} F(v_1 t')] [E_1(w_2' t') - E_1(w_2'' t_2')] + \frac{\tilde{n}_1}{q s_2} \{ [q - F(v_1 t')] [F(w_2'' t') - F(w_2' t')] + F(w_2'' t') \ln(w_2'' t') - F(w_2' t') \ln(w_2' t') - u - (w_2'' - w_2') [1 - \exp(-v_1 t')] (v_1 t')^{-1} \}, \quad (21)$$

where

$$u = \begin{cases} (w_2'' t') \ln(w_2'' t') - (w_2' t') \ln(w_2' t') - (w_2'' - w_2') t', & w_2'' t' < 1 \\ 1/2 \ln^2(w_2'' t'), & w_2' t' \ll 1 \ll w_2'' t' \\ s_2 \ln[(w_2' w_2'')^{1/2} t'], & 1 \ll w_2' t'. \end{cases}$$

Comparison of the obtained equations with the experimental data at  $T = 4.2$  K is made difficult by the insufficient operating speed of the system. We have confined ourselves to the estimate  $\bar{\sigma}_2 \approx 10^{-14}$  cm<sup>2</sup>. Equations (21) will be used below to discuss the annealing of the traps.

### TEMPERATURE DEPENDENCES

The decrease of the photoconductivity with rise of temperature was illustrated in Fig. 2. These data pertain to the value of  $G_1$  at  $t_1 = 20$  min. If we plot the value of  $G_2$  after relaxation in darkness for a fixed time  $t_R = 20$  min, we obtain a similar curve, shifted somewhat in the ordinate direction. Let us dwell now on the analysis of the experimental data obtained by solving the kinetic equation. The equations of the preceding sections were used to analyze the primary-illumination and relaxation curves plotted at intermediate temperatures. Figure 15 shows the temperature dependences of the parameter  $w_1' = I\sigma_1'$  determined by a procedure exemplified in Fig. 10. According to our model, Fig. 15 yields the temperature dependences of the right-hand edge of interval of the cross sections  $\sigma_1'$ . We recall once more that in the derivation of our equations we neglected completely the recombination of the secondary centers, a procedure apparently valid for  $T \lesssim 50$  K.

Ridley's monograph<sup>21</sup> contains an expression for the cross section of photoionization of a filled  $p$ -orbital of a deep center:

$$\sigma_T = \alpha a_H^2 \left( \frac{R_H}{\hbar\omega} \right) \left( \frac{p_{cv}^2}{2m_0} \right) \left( \frac{2m^*}{\hbar^2} \right)^{1/2} E_k^{1/2} \frac{V_T}{\eta}. \quad (22)$$

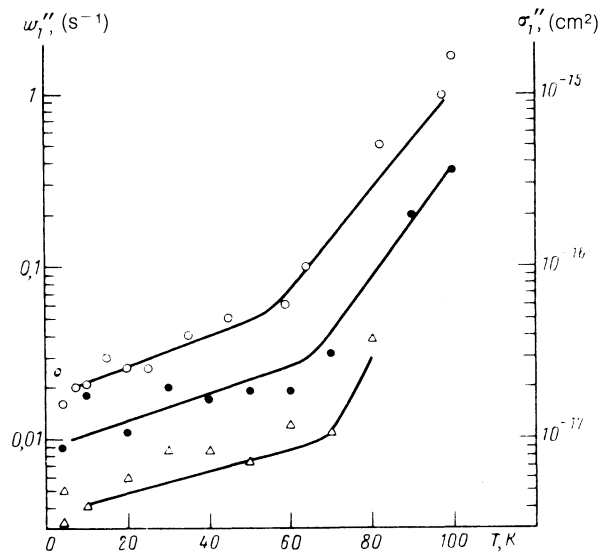


FIG. 15. Dependence of the parameter  $w_1' = I\sigma_1'$  and of the maximum cross section  $\sigma_1''$  of the primary illumination on the temperature  $T$  for samples 1 (○), 2 (●), and 3 (△). The solid curves are approximations.

Here  $\alpha = e^2/\hbar c = 1/137$  and  $a_H = \hbar^2/m_e^2$ , so that  $\alpha a_H^2 = 2 \cdot 10^{-19}$  cm<sup>2</sup>;  $R_H = e^2/2a_H$  is the Rydberg constant,  $\hbar\omega$  is a photon energy such that  $(R_H/\tau\bar{\omega}) \approx 10$ ;  $p_{cv}$  is the interband momentum matrix element, so that  $(p_{cv}^2/2m_0) \sim 0.5$  eV;  $(2m^*/\hbar^2)^{3/2} E_k^{1/2} \approx 10^{21}$  eV<sup>-1</sup>·cm<sup>-3</sup> is the characteristic density of states in the band;  $\eta = 6$  is the refractive index of PbTe;  $V_T \approx r_T^3 \approx 10^{-21}$  cm<sup>3</sup> is the effective localization volume of the electron wave function on a deep center, and  $r_T$  is the localization radius. Taking into account all the numerical values of the parameters, we obtain from (22) an estimate  $\sigma_T \approx 10^{-18}$  cm<sup>2</sup> for the photoionization cross section. Equation (22) is an estimate, in which the matrix element  $p_{cv}$ , the density of states, and the radius  $r_T$  are particularly indeterminate. The agreement between the theoretically estimated  $\sigma_T$  and the experimental  $\sigma_1'$  seems therefore quite satisfactory. It remains unclear which factor in (22) causes the small increase of  $\sigma_1'$  when the temperature and the scatter of  $\sigma_1'$  are increased on going from one sample to another.

Figure 16 shows the temperature dependence of the factor  $I\bar{\sigma}_2$ , which yields the cross section  $\bar{\sigma}_2$  for trap photoionization. On the average we have  $\bar{\sigma}_2 = 10^3 \sigma_1'$ , but in some cases, for example for sample No. 1 at  $T \approx 50$  K, we have a ratio  $\bar{\sigma}_2/\sigma_1' \approx 10^4$ . According to Eq. (22), so large a ratio of the cross sections means that the trap-localization radius is  $r_T' = (10-20)r_T$ , where  $r_T$  is the localization radius of the primary centers. We arrive thus at  $r_T' \approx 200$  Å, which agrees with the dimension of the  $p$  regions on the sample microphotographs. However, the temperature dependence and the large changes on going from sample to sample show that  $\bar{\sigma}_2$  is not simply a photoionization cross section of a well defined and reproducible object. Obviously, the fluctuations of the random potential alter  $\bar{\sigma}_2$  strongly.

Figure 17 shows the temperature dependences of  $\tau_2$ , which also reflect the characteristics of the random potential relief. This pertains here to the dynamics of the localization

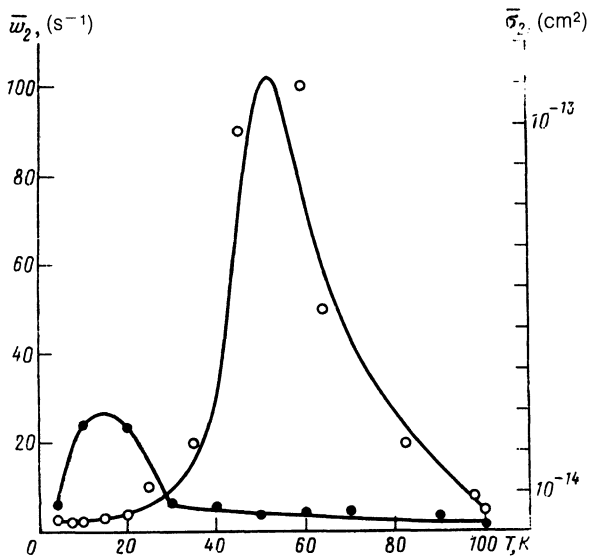


FIG. 16. Temperature dependence of the parameter  $\bar{w}_2 = I\bar{\sigma}_2$  ( $\sigma_2 = (\sigma_2' \sigma_2'')^{1/2}$ ) for samples No. 1 (O) and 2 (●). The value of  $w_2$  was determined by fitting Eq. (18) to the experimental relaxation curves in the interval  $t_R \sim 10^3$  s. The solid curves are approximations.

processes. The quantity  $q = 2(2m^* \delta U)^{1/2} D / \hbar$  is in fair agreement with the estimates  $\delta U \approx 0.1$  eV and  $D = 300$  Å, as already illustrated above. Somewhat surprising is the stabilization of  $\tau_2$  on a constant level when the temperature rises to  $T > 40$  K. It might seem that thermal excitation should facilitate access to all traps and accelerate the relaxation thereby. It is possible that a certain dynamic equilibrium is established in the filling and depletion of the traps. The kinetic equation (7) shows no term describing a thermal depletion of traps.

In conclusion, we turn to the temperature dependence of the density  $n_0$  of optically active frozen-in photoconduc-

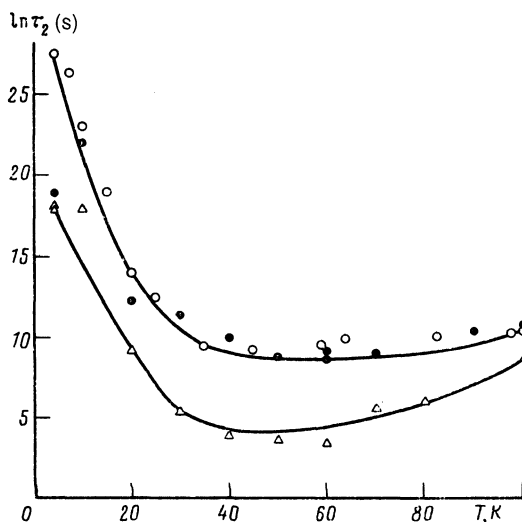


FIG. 17. The parameter  $\tau_2 = \tau_1 e^q$ , determined by the best fit of the relaxation curve to Eq. (18) at various temperatures for samples No. 1 (O), 2 (●), and 3 (Δ).

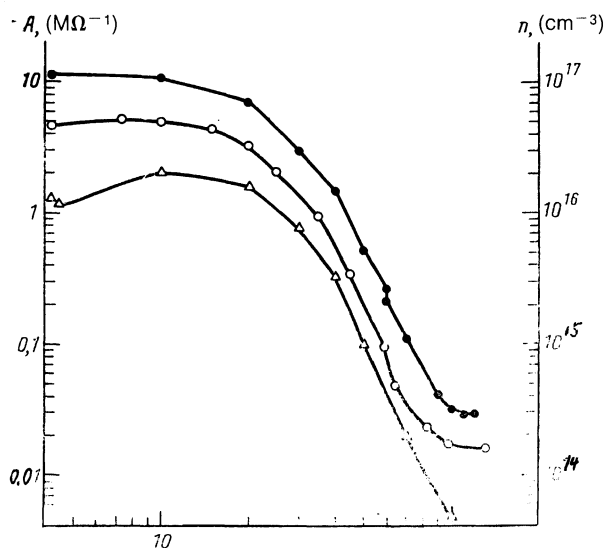


FIG. 18. Normalization coefficient  $A$  determined by comparing Eq. (13) with the experimental primary-illumination curves of Fig. 10. The density  $n$  of the primary centers was calculated using the Drude formula with  $l = 1$  Å. Symbols: O—specimen No. 1, ●—No. 2, Δ—No. 3. The solid curves are approximations.

tivity. According to Figs. 2 and 18,  $n_0$  decreases strongly with rise of temperature. Recall that we defined as the primary center a localized state of electrons on an  $O^{2-}$  impurity. The energy of this level, including the lattice-deformation energy, was designated  $E_1$  in Fig. 9. After photoionization and transition of the electrons to the conduction band ( $E_0$  curve in Fig. 9) the electron-localization energy level  $E_0^*$  at the secondary (neutral) center becomes higher than  $E_f$ , and the activation energy for thermally stimulated recombination of secondary centers into primary is  $\tilde{U} \approx 0.1$  eV. Clearly, the different impurity atoms can have a large scatter of  $E_0^*$ . Some of the  $E_0^*$  may turn out to be lower than  $E_f$  and produce no long-lived free carriers. Figure 18 shows the temperature dependences of the fit parameters  $A$  for primary illumination at intermediate temperatures. According to (11) and (12), this coefficient is proportional to  $n_0$ . It is clear from an analysis, based on solution of the kinetic equations, of the experimental data that the decrease of  $A$  by almost three orders when the temperature rises from 10 to 100 K cannot be attributed to a shortening of the relaxation time.

In our earlier paper<sup>24</sup> we attempted erroneously to attribute the decrease of  $A$  to the temperature dependence of the time of nonradiative capture of free carriers. Additional experiments, however, have shown incontrovertibly that we are dealing here not with the dynamics of photoionization and with trapping, but with the state of the specimen at a given temperature regardless of prior illumination. In the experiment, the specimen in a holder was placed above the level of liquid helium. An automatically regulated heater maintained  $T = \text{const}$  accurate to  $\sim 0.1$  K. The temperature was measured with a germanium resistor and recorded simultaneously with the film conductivity  $G$ . This yielded the  $G(T)$  plots shown in Fig. 19.

The specimen was illuminated at  $T = 4.2$  K from a state with dark conductivity  $G_d < 10^{-5} \text{ M}\Omega^{-1}$ . After relaxation

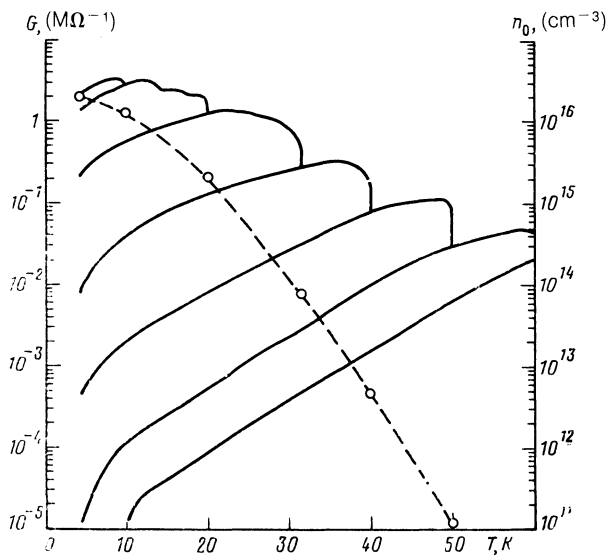


FIG. 19. Photoconductivity  $G$  of specimen No. 4 illuminated at  $T = 4.2$  K, with alternation of heating to intermediate temperatures  $T_i = 10, 20, \dots, 60$  K and cooling to 4.2 K. With  $T_i = \text{const}$  ( $i = 1, \dots, 6$ ) maintained constant for  $t_R = 20$  min. The points corresponding to a density  $n_0$  in the scale of the right-hand ordinate axis, calculated from the value of the conductivity using the Drude formula with  $l = 1 \text{ \AA}$ .

for 20 minutes the conductivity decreased by  $\sim 30\%$ . This value  $G_2(4.2 \text{ K}) \approx 2 \text{ M}\Omega^{-1}$  is marked by a point on Fig. 19. The specimen was then heated to  $T_i = 10, 20, \dots, 60$  K, where  $i = 1, 2, \dots, 6$ . Relaxation for  $t_R = 20$  min was produced at each temperature  $T_i = \text{const}$ . These vertical sections are clearly seen in Fig. 19. After relaxation at  $T = T_i$ , the sample temperature dropped to  $T_0 = 4.2$  K, and then returned to the value  $T_i$ . It took several minutes to immerse the specimen in liquid helium, and then raise and heat it. The  $G(T)$  curves obtained by cooling and then heating were therefore practically the same. It was clear at the same time that a return to the initial relative relaxation rate  $d(\ln G_2)/dt$  requires a time interval  $t_R \sim 20$  min after each rise of temperature from  $T_i$  to  $T_{i+1}$ . In the concluding stage the specimen was heated to  $T \gtrsim 150$  K and illuminated from the dark state after cooling to  $T = T_i$  and relaxed for 20 minutes.

The obtained values of  $G_2$  agreed accurate to  $\approx 50\%$  with the ends of the relaxation sections in Fig. 19. This gave rise to our statement that the sample state is a function of temperature regardless of the prior history. We assume that the corresponding function of state is the density of the primary centers. Although the oxygen density is fixed, the positions of the levels  $E_g^*$  on the energy scale relative to  $E_f$  can vary with temperature for the same reasons as the band gap  $E_g$  in PbTe crystals. It is interesting that if the cooling and heating cycle is interrupted, and after relaxation at some arbitrary temperature  $T_i > 20$  K the specimen is cooled to 4.2 K at which it is kept for a long time ( $\sim 24$  hours), the traps filled at the temperature  $T_i$  are slowly depleted and the conductivity  $G$  increases slowly but remains considerably lower than  $G_2(T_i)$ . At the present time the mechanism of the temperature shifts relative to the level positions in PbTe has not yet fully determined, although computation results are available for  $E_g$  (Refs. 25, 26).

The conductivity values  $G(4.2 \text{ K})$  obtained after an  $i$ th relaxation are marked on Fig. 19 at points with the abscissa  $T = T_i$ . We took thereby into account the factor  $\exp[(E_f - E_p)/k_B T]$  that determines the temperature dependence of the conductivity in a random potential (see Fig. 3). The points on Fig. 19 describe therefore the temperature the  $n_0(T)$  dependence proper. The scale of the  $n_0(T)$  plot shown on the right-hand ordinate axis was determined from the conductivity values by the Drude formula, with a minimum carrier free path  $l = 1 \text{ \AA}$  in accordance with Mott's concept of minimal metallic conductivity.

## ANNEALING OF LOCALIZED STATES

The results shown in Fig. 16 indicate that sample No. 1 distinctly revealed at  $T = 50$  K an increase of the cross section  $\bar{\sigma}_2$  for secondary illumination. From Eq. (22) we have  $\sigma_2 \propto r_T^3$ . Thus, under conditions of continuous optical excitation, the localization of the nonequilibrium carriers proceeds to states with large  $r_T \approx 200 \text{ \AA}$ . Of course, the many traps include also states with lower  $r_T$ , but their number is relatively small. We have organized experiments in which the temperature dependence of  $r_T$  was investigated without continuous optical excitation.

The experiments comprised series of alternating relaxation and second-illumination processes at  $T = T_0 = 4.2$  K. During time of relaxation in darkness, the specimen temperature was raised to some intermediate value  $T = T_i$  and was then returned to  $T = 4.2$  K. The total thermal cycle lasted  $\approx 2$  min, and the specimen temperature was  $T = T_i$  for  $\approx 1/2$  min. This intermediate annealing altered substantially the  $\sigma_2$  distribution of the traps. In the absence of annealing or at low annealing temperature,  $T_i < 30$  K, the secondary-illumination curve was poorly described by our approximate solution of the kinetic equation, but a sufficiently reliable estimate could be obtained for the right-hand edge of the interval  $\sigma_2''$  and for the logarithmic width of the distribution  $s_2 = \ln(\sigma_2''/\sigma_2')$ . At high annealing temperatures  $T_i > 40$  K the agreement between the experimental curves and Eqs. (21) was good. In Fig. 20 the discrepancy between theory and experiment is manifested by a deviation of the dashed line from a straight one. The initial and final points are fixed by the continuous experimental curves. The fit parameters are determined with good accuracy, within  $\lesssim 10\%$ . The results shown in Fig. 21 were obtained in this fashion.

To prevent misunderstandings, we note the following. Assume, as an abstract example, a group of certain photosensitive centers having a density  $n$  and a cross section  $\sigma$ . The derivative  $\dot{G}|_{t=0} \propto I\sigma n$  of the photoresponse at the start of the illumination is determined both by the cross section and by the density of the center. After a certain time  $t_f$  the photoresponse  $G$  assumes a stationary value. Neglecting recombination we have  $t_f = (I\sigma)^{-1}$ , but at any rate the time constant  $t_f$  does not depend on the density  $n$ . In our case everything is made more complicated in view of the distribution of the centers with respect to the cross sections  $\sigma_2$ . Nonetheless, the procedure for estimating  $\sigma_2'$  and  $\sigma_2''$  from the characteristic times of the start and end of the logarithmic section yields just the cross sections  $\sigma_2$  and is independent of the density. Analysis of the temperature dependence

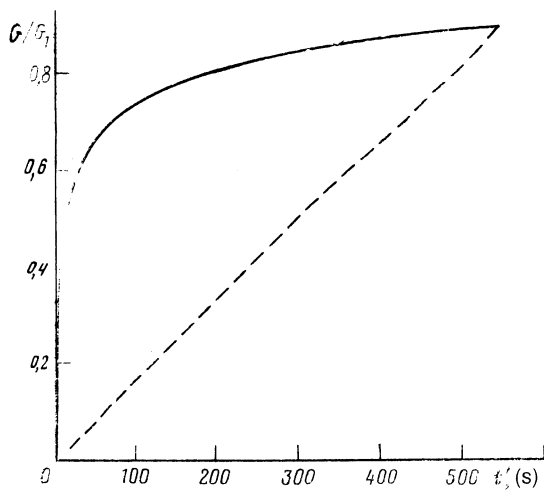


FIG. 20. Comparison of theory with experiment (continuous curve) for secondary illumination of specimen No. 2 at  $T = 4.2$  K after intermediate annealing in darkness at  $T = 60$  K. The abscissa for the dashed curve is not  $t'$  but  $\xi$  which is equal to the expression in the curly brackets in Eq. (21), corresponding to the condition  $n_2 = 0$ . The proportionality coefficient in the relation  $G \propto \xi$  was chosen to cause the continuous and dashed curves to meet at the extreme right-hand point. The parameters are  $w_2'' = 1.6 \text{ s}^{-1}$ ,  $w_2' = 1.1 \cdot 10^{-3} \text{ s}^{-3}$ .

of  $G(t')$  in the course of the secondary illumination after an intermediate annealing shows that under reasonable assumptions the observed curves attest not to a decrease of the density of the secondary centers, but just the decrease of the cross sections  $\sigma_2'$  and  $\sigma_2''$  with rise of the annealing temperature. This conclusion is not connected with any specific distribution function ( $dn/d\sigma_2 \propto \sigma_2^{-1}$ ), but has a more general justification of the same type as the time constant of the illumination for a simple group of centers.

A curious picture of thermal annealing of localized states is thus observed. The relaxing nonequilibrium carriers captured in metastable traps having a large capture cross section find energywise favorable states whose radius  $r_T$  decreases continuously with rise of the annealing temperature. This consequence is undisputable evidence of the localization singularities, which we ascribe to Anderson localization conditions, in a random potential  $\delta U$ . The trapping centers are not isolated defects with definite discrete states, but a coherent state superposition whose characteristic radius decreases continuously as barriers of various scales are overcome by thermal activation in the potential  $\delta U$ .

Figure 21 shows the decrease of  $\sigma_2''$  to almost  $\sigma_1 \lesssim 10^{-3} \sigma_2''$ . The logarithmic parameter  $s_2$  of the distribution width should have also increased at least to the lower limit  $s_1 > 10$ . We assume that the solution obtained for the kinetic equation (21) without allowance for recombination of the secondary centers and their return to the primary state leads to an incorrect estimate of the distribution width  $s_2$  at  $T_i > 80$  K. This conclusion, however, does not devalue the data obtained at lower intermediate-annealing temperatures. The procedure described permits a new approach to the possibility of investigating the Anderson localization. Of greatest interest would be primary and secondary illuminations at different light-source wavelengths.

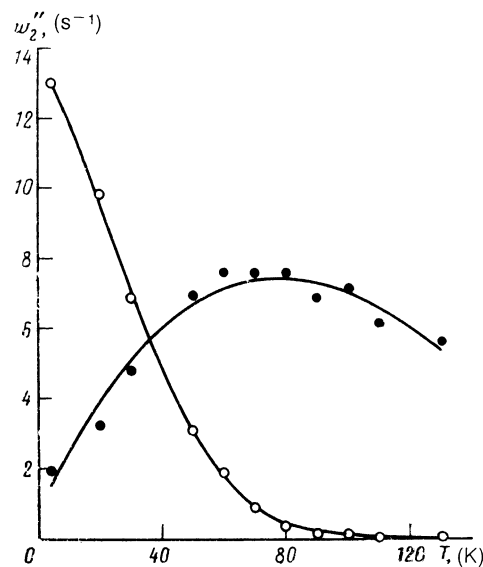


FIG. 21. Secondary-illumination parameters  $w_2'' = I\sigma_2''$  (O) and  $s_2 = \ln(\sigma_2''/\sigma_2')$  (●) vs the annealing temperature  $T$ . Sample No. 2, primary and secondary illuminations at  $T = 4.2$  K. Annealing in darkness between the illuminations. The ordinate scales correspond to  $[w_2''] \text{ s}^{-1}$  for the points O and are dimensionless for ●.

## CONCLUSION

We have investigated a group of phenomena connected with long-time photoconductivity in oxidized PbTe:O films at low temperatures  $T < 100$  K. It was established by using secondary illumination that as a result of lattice deformation the deep levels of electrons localized on defects, presumably doubly charged  $\text{O}^{2-}$  ions, acquire higher energy. Recombination of conduction electrons and unfilled centers is a thermoactivated process with activation energy  $\tilde{U} \approx 0.1$  eV. A lower limit  $\tau_T > 10^6$  s was established for the recombination time constant at  $T = 4.2$  K. The existence of "frozen-in" centers is attributed to strong vibronic interaction in the PbTe lattice. Photo-deionization of the  $\text{O}^{2-}$  impurity deforms the PbTe:O lattice near the defect. Part of the lattice-deformation energy serves as an energy barrier that hinders the electron localization on the defect and the return of the center to the initial state.

Measurement of the time dependences of the specimen conductivity  $G$  during illumination and relaxation has shown that the photoexcited carriers become trapped. We solved an illumination kinetic equation in which the initial parameters were the photoexcitation cross sections  $\sigma_1$  of the impurities and  $\sigma_2 \gg \sigma_1$  of the traps, and also the time  $\tau$  to trap the conduction electrons. Analysis of the solution has shown that a description of experimental dependences of type  $\Delta G \propto \log t$  calls for introduction of a large set of cross section in the ranges  $\sigma_1' \leq \sigma_1 \leq \sigma_1''$ ,  $\sigma_2' \leq \sigma_2 \leq \sigma_2''$ , and of time constants  $\tau_1 \leq \tau \leq \tau_2$ . The distribution functions are then  $dn/d\sigma \propto \sigma^{-1}$  and  $dn/d\tau \propto \tau^{-1}$  and the logarithmic factors of the distribution widths are  $s_1 = \ln(\sigma_1''/\sigma_1') \gg 1$  and  $q = \ln(\tau_2/\tau_1) \gg 1$ . Parameter values  $\sigma_1'' = 10^{-17} \text{ cm}^2$ ,  $\tau_1 = 10^{-4} \text{ s}$ , and  $\tau_2 = 10^{12} \text{ s}$  at  $T = 4.2$  K were established. These results agree with theoretical estimates of the cross sections for photoionization and capture by deep centers, and also with estimates of the tunneling transparency of the random-potential

barriers in doped and compensated PbTe:O films.

The substantial role of strong-disequilibrium photoexcited electrons was established by the method of bilateral second illumination. It seems that in PbTe:O films of thickness  $d \gtrsim 1000 \text{ \AA}$  the electron delocalization from deep levels and traps is due mainly to impact by electrons excited by photons of energy  $\hbar\omega \approx 2 \text{ eV}$  near the specimen surface. The large value of  $s_1$  is presumably due to the broad energy spectrum of the nonequilibrium electrons and to the strong energy dependence of the cross section for impact ionization of the impurities and traps.

Doping and compensation fluctuations in the course of specimen preparation produce randomly alternating  $p$ - $n$  junctions, i.e., a random relief of the electron potential energy is produced. As a result, the conditions in our experiments are more complicated than in the original Anderson localization model. Beside the scatter of the energy eigenvalues  $\varepsilon_i$  of the individual levels, which can be called in the language of the second-quantization Hamiltonian "diagonal" disorder, i.e., scatter of the values of the matrix elements of the transition between the states  $\varepsilon_i$  in view of the large variations of the tunnel transparency of the barriers. In addition, a theoretical development of a model for localization in PbTe:O is made complicated by vibronic interaction.

From the experimental standpoint, development of a second-illumination procedure has factually uncovered a new approach to the study of the Anderson localization. Solution of the kinetic equation has made it possible to relate the time dependence of the specimen conductivity in relaxation second-illumination processes with the average photoionization cross sections  $\bar{\sigma}_2 = (\sigma'_2 \sigma''_2)^{1/2}$  of the traps and with the boundaries  $\sigma'_2 \leq \sigma_2 \leq \sigma''_2$  of the interval. In the well-developed theory of photoionization of deep centers in semiconductors, the value of  $\sigma_2$  is determined by the volume of the region of electronic-state localization, i.e., is a characteristic of the spatial scales of the superposition of states in the Anderson-localization model. In contrast to a simple single trap, where the subject is a defect of radius  $r_T \approx a \approx 10 \text{ \AA}$ , in the case of Anderson localization in a random potential the states are formed via many unit cells and the localization radius  $r_T$  becomes a mesoscopic quantity. A localized state is not a state of a discrete spectrum with well-defined value of  $\sigma_2$ . In addition to the properties of the defect and of its nearest surrounding, the value of  $\sigma_2$  is determined by the measurement procedure and by the experimental conditions.

In our experiments we measured at  $T = 4.2$  the characteristic value  $\bar{\sigma}_2 \approx 10^{-14} \text{ cm}^2$  which, compared with the experimental value  $\sigma''_1$ , provides an estimate of the volume  $V_T \sim 10^3 a^3$  of the localized state and of the radius  $r_T \approx 100 \text{ \AA}$ . It was shown by using the intermediate-annealing method that the maximum second-illumination cross section decreases smoothly with rise of the annealing temperature  $T_i$  and tends at  $T_i > 100 \text{ K}$  to the value  $\sigma''_1$  typical of the initial

deep centers. This experimental result is, in our opinion, the clearest manifestation of the specific features of the Anderson localization as compared with trapping by an individual trap.

The use of the methods developed here, in conjunction with variation of wavelength of the light, makes it possible to extract much more complete information on localization processes in a random potential. Obvious possible applications of the freezing-in photoconductivity involve the study of the energy loss by electron excitations propagating in metal and semiconductor films, and also the development of system of image recording at low temperatures.

The authors thank A. F. Andreev and A. Ya. Parshin for a discussion of the results, Ya. B. Poyarkov for many years of fruitful collaboration, and M. S. Tyurin for constant help with the organization of the experiments.

<sup>1</sup> We thank A. M. Gas'kov and V. I. Shtanov for collaboration.

<sup>1</sup> I. P. Krylov and V. E. Nadgronyi, *Pis'ma Zh. Eksp. Teor. Fiz.* **35**, 56 (1982) [JETP Lett. **35**, 65 (1982)].

<sup>2</sup> H. J. Queisser, *Proc. 17th Conf. on Semicond.*, J. Chadi and W. Harrison, eds., San Francisco, 1984, p. 1303.

<sup>3</sup> M. K. Sheinkman and A. Ya. Shik, *Fiz. Tekh. Poluprov.* **10**, 209 (1976) [Sov. Phys. Semicond. **10**, 128 (1976)].

<sup>4</sup> D. V. Lang and R. A. Logan, *Phys. Rev. Lett.* **39**, 635 (1977).

<sup>5</sup> G. Nimtz, Landolt-Boernstein, *New Series, Group III*, Springer, 1983, Vol. 17f, p. 170.

<sup>6</sup> G. Nimtz and B. Schlicht, *Narrow Gap Lead Salts*, Springer, 1983.

<sup>7</sup> V. A. Volkov and O. A. Pankratov, *Zh. Eksp. Teor. Fiz.* **88**, 280 (1985) [Sov. Phys. JETP **61**, 164 (1985)].

<sup>8</sup> N. Parada and G. Pratt, *Phys. Rev. Lett.* **22**, 180 (1969).

<sup>9</sup> V. A. Volkov and O. A. Pankratov, *Dokl. Akad. Nauk SSSR* **255**, 93 (1980) [Sov. Phys. Doklady **25**, 922 (1980)].

<sup>10</sup> B. M. Vul, I. D. Vornova, G. K. Kalyuzhnaya *et al.*, *Pis'ma Zh. Eksp. Teor. Fiz.* **29**, 21 (1979) [JETP Lett. **29**, 18 (1979)].

<sup>11</sup> B. A. Akimov, N. B. Brandt, S. A. Bogoslovskii *et al.*, *ibid.* **29**, 11 (1979) [JETP Lett. **29**, 9 (1979)].

<sup>12</sup> I. I. Zasavitskii, B. M. Matsionashvili, O. A. Pankratov, and V. G. Trofimov, *ibid.* **42**, 3 (1985) [JETP Lett. **42**, 1 (1985)].

<sup>13</sup> J. Baars, Landolt-Bornstein, *New Series, Group III*, Springer, Vol. 17d, p. 251 (1983).

<sup>14</sup> Ya. B. Poyarkov, Candidate's dissertation, Inst. Phys. Problems, Moscow (1989).

<sup>15</sup> I. P. Krylov and B. E. Nadgornyi, *Pis'ma Zh. Eksp. Teor. Fiz.* **34**, 186 (1981) [JETP Lett. **34**, 178 (1981)].

<sup>16</sup> D. L. Bode and H. Levinstein, *Phys. Rev.* **96**, 259 (1954).

<sup>17</sup> N. F. Mott and M. Kaveh, *Adv. Phys.* **34**, 39 (1985).

<sup>18</sup> T. Moss, *Optical Properties of Semiconductors*, Butterworths, 1959.

<sup>19</sup> D. Lang, in *Deep Centers in Semiconductors*, S. Pantelides, ed., Gordon & Breach, 1986, p. 489.

<sup>20</sup> V. Cochran, *Phys. Rev. Lett.* **13**, 193 (1964).

<sup>21</sup> B. K. Ridley, *Quantum Processes in Semiconductors*, Oxford Univ., N.Y. (1982).

<sup>22</sup> M. Abramowitz and I. A. Stegun, *Handbook of Mathematical Functions*, Dover, 1964.

<sup>23</sup> I. P. Krylov, *Phys. Rev. B* **38**, 7800 (1988).

<sup>24</sup> K. A. Baklanov and I. P. Krylov, *Pis'ma Zh. Eksp. Teor. Fiz.* **48**, 330 (1988) [JETP Lett. **48**, 364 (1988)].

<sup>25</sup> W. M. Anderson, *IEEE J. QE* **13**, 532 (1977).

<sup>26</sup> Y. W. Tsang and M. L. Cohen, *Phys. Rev. B* **3**, 1254 (1971).

Translated by J. G. Adashko